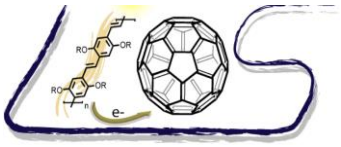

JOHANNES KEPLER
UNIVERSITY LINZ

Submitted by

Corina Schimanofsky

Submitted at

Institute of Physical Chemistry and Linz Institute of Organic Solar Cells

Supervisor

Prof. Niyazi Serdar Sariciftci

Co-supervisor
Dominik Wielend

September 2021

(SPECTRO)ELECTROCHEMICAL INVESTIGATION OF ANTHRAQUINONE DERIVATIVES UNDER CO_2 AND O_2

Bachelor Thesis

to obtain the academic degree of

Bachelor of Science (BSc)

in the Bachelor's Program

Chemistry and Chemical Technology

STATUTORY DECLARATION

I hereby declare that the thesis submitted is my own unaided work, that I have not used any sources other than those indicated and that all direct and indirect sources are acknowledged as references.

This printed thesis is identical with the electronically submitted version.

Place, Date Signature

Acknowledgment

First and foremost, I would like to thank o.Univ. Prof. Mag. Dr. DDr. h.c. Niyazi Serdar Sariciftci, who offered me the great opportunity of being part of the LIOS team.

A special thank you to my co-supervisor DI Dominik Wielend who raised my interest in electrochemistry and supported me with advice and action during my whole time at the institute. Without him this work would not look the way it does now.

I also would like to thank Dr. Helmut Neugebauer for his time and open ear when electrochemical questions arose.

Furthermore, I would like to thank the whole LIOS team for their warm welcome, their support, advice and help whenever it was needed. A special thank you to Dr. Mihai Irimia-Vladu for providing the used materials, and to DI Felix Mayr for his help with the PL measurements.

Finally, I would like to thank my family and friends who have always supported me, always had an open ear and tried to understand my interest in this subject.

Abstract

Due to the present topics of climate change and global warming the interest and request in CO_2 reduction and capturing as well as in renewable energy and energy storage methods increased. In this work the topics of CO_2 capturing as well as O_2 reduction are discussed. Both topics were studied electrochemically in solutions having homogeneously dissolved anthraquinone (AQ) derivatives. AQ and its derivates were chosen as material class, as they are known as catalysts for electrochemical as well as chemical processes.

The first part of this thesis deals with the optical characterization of the used AQs through infrared (IR), UV-vis, as well as photoluminescence (PL) spectroscopy and approaches the question if and how homogeneously dissolved AQs are able to reduce or capture CO_2. In order to approach this task, the methods of electrochemical cyclic voltammetry (CV) and spectroelectrochemistry under N_2 and CO_2 were used.

The second part covers the topic of oxygen (O_2) reduction to hydrogen peroxide H_2O_2, again using homogeneously dissolved AQs as electrocatalysts. Here, the methods of CV and chronoamperometry were used to characterize the oxygen reduction and quantify the moles of H_2O_2 produced. The experiments were performed in aqueous as well as in non-aqueous solution in acetonitrile (MeCN).

Contents

1. Introduction

Since the industrial revolution the approximately 80 % of the world's energy needs is provided by technologies based on fossil hydrocarbons. Due to a growth in the world's population the required amount of energy increased. A consequence of the combustion of the fossil fuels is the increase of greenhouse gases, especially CO_2 [1]. The rise in the CO_2 concentration in the atmosphere causes consequences like climate change and global warming, as well as further environmental reactions [2]. If the increase of CO_2 is not hindered and reduced the earth crust will heat up further and the water level will rise. Nowadays, the side effects can be clearly and dramatically seen. For instance the heating of the earth crust as well as the following rise of the water level [3] result in a reduction of agricultural production[4], an increase of forest fires, floods as well as in a decreasing ability for fresh water [2]. However, energy has an important role, and it is necessary to find an alternative way for renewable energy generation with less CO_2 emission. Therefore, the focus is on alternative/renewable energy, as well as energy storage [2,5].

Renewable energy is generated from resources again and again without/with less harmful by-products. Main sources for renewable energy are for instance: hydropower, solar energy, wind energy [6], and hydrogen [5]. A difference between renewable energy and fossil fuels is the availability. While fossil fuels are permanent available and easy storable if they are not needed, renewable energy has to be harvested when they are available and stored until they were needed. Different methods of storage are available depending on the type of the to be stored energy. Energy can be stored for instance electrochemically in batteries, or capacitors [7]. The storage of renewable energy is only possible to a certain degree. With this method, energy cannot be stored economically enough to supply an entire city with energy. For this purpose renewable fuels like CH_4 or CO produced from CO_2 are a better alternative.

1.1 Role of CO_2

In the last few decades a rise of pollutants was noticeable in the atmosphere. The increase of CO_2 is due to industrialization and urbanization[8]. A further reason for the rise of the greenhouse gas concentration of CO_2 in the atmosphere is attributable to the increasing use of fossil fuels for electricity, agricultural production, and transportation [9]. Especially, the high CO_2 emission leads to global warming as well as to climate change[10]. Consequences of these are for instance low rain periods, higher temperatures, and fluctuations in season [8,11]. To counteract the consequences of global warming and climate change the CO_2 emission has to be decreased. Therefore, each country tries to reduce their CO_2 emission. Methods like using renewable energy, avoiding the use of fossil fuels, and sustainable economic growth are used[12].

To achieve the goal of CO_2 reduction, Carbon Capture and Utilization (CCU) is an attractive method. A reason for this is not only the reduction of the emission but also the creation of

useful products. So, CO_2 is used as a starting material. Some processes like carbonisation of beverage, the direct use in refrigeration systems, and fire extinguisher are already developed and widely used. Other fields of applications are currently under development [13]. In general, it is not guaranteed that the use of CO_2 as starting material is environmentally friendly. Since energy and highly energetic co-reactants were used, indirect CO_2 is produced in certain processes [13].

Another method for reduce the CO_2 emission is Carbon Capturing and Storage (CCS). In the industrial sector CCS is considered as the only method for reducing the CO_2 emission, if the replacement of material and/or process is not possible [13]. CCS includes the following four steps: capture, conditioning, transportation, and storage. There are two possibilities for CO_2 storage (geological storage and ocean storage) [13,14].

To decrease the CO_2 percentage in the atmosphere many researches in the field of CCS, CCU, as well as CO_2 reduction, and in the area of renewable energy were carried out [15,3]. Some LIOS members were also working on these topics. This already existing research includes: Capture and release of CO_2 in aqueous solution with an organic semiconductor electrode [16], CO_2 reduction in non-living bioanalyzed reactions with enzymes [17], or in homogeneous and heterogeneous catalytic approach using organic and organometallic as well as bioorganic systems [18]. They also carried out experiments for a controlled capture and release in a heterogeneous system with quinacridone [19] as well as with anthraquinone [20]. Therefore, the focus of the following study was laid upon AQs in homogenous solution in order to add to the findings of the already existing studies from this institute. AQs in homogeneous systems have already been discussed in existing literature, for example in Yin et al. (2018) [21], Gurkan et al. (2015) [22], and Tam et al. (2021) [23].

1.2 Electrochemical background of oxygen reduction

In oxygen electrochemistry there are oxygen reduction and oxygen evolution. In Oxygen reduction reaction (ORR) a product is formed through receiving an electron while in oxygen evolution reaction (OER) molecular oxygen is generated via oxidation of water[24]. ORR is a well studied electrochemical reaction due to its importance in energy conversion and storage [25] as well as in practical technologies and industrial processes [24].

Hydrogen peroxide (H_2O_2) which is produced in ORR can be the final product as well as an intermediate [26]. For ORR different pathways exist. The four electron transfer reaction is the thermodynamically favoured pathway to produce H_2O at a standard potential of 1.23 V vs. SHE [26].

$$O_2 + 4H^+ + 4e^- \rightarrow 2H_2O \qquad \text{Eq. 1}$$

Furthermore, there is a 2 e^- reduction which produces H_2O_2 as an intermediate which is then further reduced to H_2O. While the reduction to H_2O_2 takes places at a potential of 0.67 V the reduction to H_2O takes place at 1.77 V [25,26].

$$O_2 + 2H^+ + 2e^- \rightarrow H_2O_2 \quad \text{Eq.2}$$

$$H_2O_2 + 2H^+ + 2e^- \rightarrow 2H_2O \quad \text{Eq.3}$$

If a direct 4 e^- reaction to H_2O or a 2 e^- reduction to H_2O_2 is performed can depend on the material of the electrode. While Pt electrodes tend to a the 4 e^- pathway, a gold and mostly all carbon-based electrodes tend to produce H_2O_2 [27,28]. Generally, the electrochemical production of H_2O_2 is considered as an environmentally friendly way. Instead of hazardous reactants a "green" reactant the electron is used. Furthermore, purification of the product is not required [29]. This method, which is used on a large-scale, is described more accurate in chapter 1.3 .

Hydrogen peroxide is not only able to accept an electron in reduction processes. It is also able to donate electrons in oxidation processes. Through disproportionation H_2O and O_2 are generated. This reaction is exactly the same as it occurs in one-compartment fuel cells containing H_2O_2 [30].

$$2H_2O_2 \rightarrow 2H_2O + O_2 \quad \text{Eq.4}$$

Here, it is important to control the reaction due to the production of gaseous oxygen and heat. The produced heat corresponds to approximately 100.4 kJ mol^{-1}. H_2O_2 decomposes to H_2O and O_2 without the production of any greenhouse gas emission [31,32].

1.3 Hydrogen Peroxide (H_2O_2)

Hydrogen peroxide (H_2O_2) is known as a strong oxidizing agent [29], disinfectant, and as bleaching agent [33]. It is an important chemical which is used in various fields. In general, it is used for instance in industry, medicine, and for the protection of the environment [34]. It has a wide field of applications and therefore it is also used for organic synthesis, in liquid fuel rocket propulsion [35] as well as in disinfectants and water purification [36].

At room temperature the compound is a colourless liquid with a density of 1.44 g cm^{-3}. H_2O_2 is miscible with water in any desired ratio. In aqueous solution it can also form salts with various metals due to its weak acidity (pk_a = 11.8). It has a boiling point of approximately 150 °C and does not form azeotropes with water. So, it can be clearly separated from each other through distillation [37]. Due to the fact that H_2O_2 is relatively unstable transportation gets difficult [38]. This is also a reason why distillation of H_2O_2 is hazardous.

1818 Jacques Thenard described H_2O_2 as "oxygenated water". Even though many other chemists generated H_2O_2 Thenard was the first one who identified it and defined a procedure [39]. He added nitric acid to barium peroxide. The process was improved through using hydrochloric acid. The resulting barium chloride was precipitated with sulfuric acid [37,39]. It was called "wet process" due to the production of aqueous hydrogen peroxide based on wet chemical processes. The following reaction equations describe the "wet process" [37].

$$BaO_2 + 2HCl \rightarrow BaCl_2 + H_2O_2 \quad \text{Eq. 5}$$

$$BaCl_2 + H_2SO_4 \rightarrow BaSO_4 + 2HCl \quad \text{Eq. 6}$$

$$BaO_2 + H_2SO_4 \rightarrow BaSO_4 + H_2O_2 \quad \text{Eq. 7}$$

After further investigations in the production of H_2O_2 one of the main industrial processes to generate hydrogen peroxide is the anthraquinone oxidation (AO) process. Generally, this multistep process cannot be considered as a green process due to the high energy consumption and the production of waste which leads to less sustainability and high production costs [32]. Nevertheless , in this process H_2O_2 is produced in a large scale [38]. In Figure 1 the reaction scheme of the process is shown.

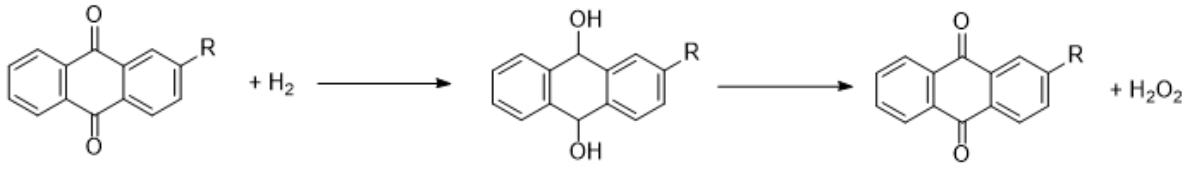

Figure 1: Reaction scheme of the anthraquinone oxidation process.

The first step in the AO process is the hydrogenation of the anthraquinone (AQ) derivative to anthrahydroquinone. In the second step the product is oxidized with O_2 to AQ and H_2O_2 is formed. The whole process is performed in an organic solvent [34] and the presence of a noble-metal catalyst. An advantage of this process is the avoidance of a direct reaction between H_2 and O_2. However, there are more disadvantages of the process like the high costs of reactants and solvents as well as the time-consuming removal of impurities and the deactivation of the hydrogenated catalyst [33]. H_2O_2 is relatively unstable and therefore it is transported in aqueous solution with added stabilizer in concentrations of 35 and 50 w%. Another method for transportation is as a stable precursor like sodium perborate or sodium percarbonate which produce H_2O_2 only in solution [32]. Nevertheless, there are further investigations in H_2O_2 production since a "greener" way of production is wanted. An alternative for the AO process is the electrochemical synthesis of H_2O_2. The disadvantage here is the difficulty for scale up [33]. An alternative for the peroxide production is the direct reaction between H_2 and O_2 acid or methanolic solution with a Au or Pd/Au alloy catalyst was investigated [35]. Due to the high explosion potential of the gaseous reactant mixture this method is not environmentally friendly. To avoid fire hazards the gases have to be diluted in CO_2 or N_2 solutions. Furthermore, a Pd catalyst is used. Nevertheless, this process is not suitable for industrial scale-up [28]. The electrochemical method is a sustainably way of H_2O_2 production and the target reaction of this work.

1.4 Anthraquinone

Generally, AQ is a tricyclic aromatic organic compound. It is classified as a quinone with the keto groups on position 9 and 10. In the solid state it is light yellow while it is colourless for the human eye in its liquid form. It has a melting point of approximately 287 °C. The compound is poorly soluble in water while it is better soluble in organic solvents. Generally, the solubility gets better with increasing temperature [40]. In Figure 2 the structural formular of AQ is shown.

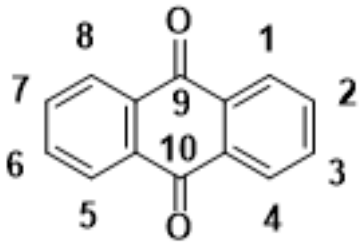

Figure 2: Chemical structure of AQ.

Through oxidation of anthracene with nitric acid the first AQ was prepared in 1868 by Laurent. Then AQ was produced through oxidation of anthracene with chromic acid by Fritzsche [41]. The compound received less attention until Graebe, and Liebermann made the groundwork of the important dye synthesis in 1838. They synthesized alizarin (1,2-Dihydroxyanthraquinone) from anthracene. Since then new dyes and acid dyes as well as vat and disperse dyes were discovered. Vat dyes are defined as molecules which can be reduced through an inorganic salt (for instance sodium thionite). Through this reduction the dye becomes soluble in water. One of the most famous vat dyes is Indigo. in general, vat dyes are used for textile colouring. Therefore, the textile is put into the reduced dye solution. For a stable colouration the dye is re-oxidized to its neutral insoluble form [42,43]. Disperse dyes belong to one of the most important groups in dye chemistry. They are used for dying hydrophobic fibres for instance polyester, nylon, and cellulose. [44] Disperse dyes are generally characterized by their low solubility in water [45].

In 1950 reactive AQs were introduced. Due to an anthracene shortage in 1970 new ways to synthesize AQ were developed. Holton discovered 1977 the catalytic effect of AQ on the alkaline pulping of wood [40]. A further use of AQs is the production of H_2O_2 via the anthraquinone oxidation process, as mentioned in chapter 1.3. AQ and its derivatives are important materials in industry as well as in medicine [46,47]. They were used for instance as laxatives or as anti-inflammatory agents [48].

Since the 18th century AQs are synthesized from anthracene. Before, this way was discovered AQs could be found in nature. This is why AQ derivatives are considered as the larges natural appearing quinones [40]. They can be found in bacteria, fungi, and insects. Whether natural or

synthetic AQs are used in pharmaceuticals, food, and cosmetics. They are also used in textile dying due to there different colours [48].

Besides the unsubstituted AQ (Figure 2) commercially available amino and/or hydroxy substituted AQs were used in this work (Figure 3)

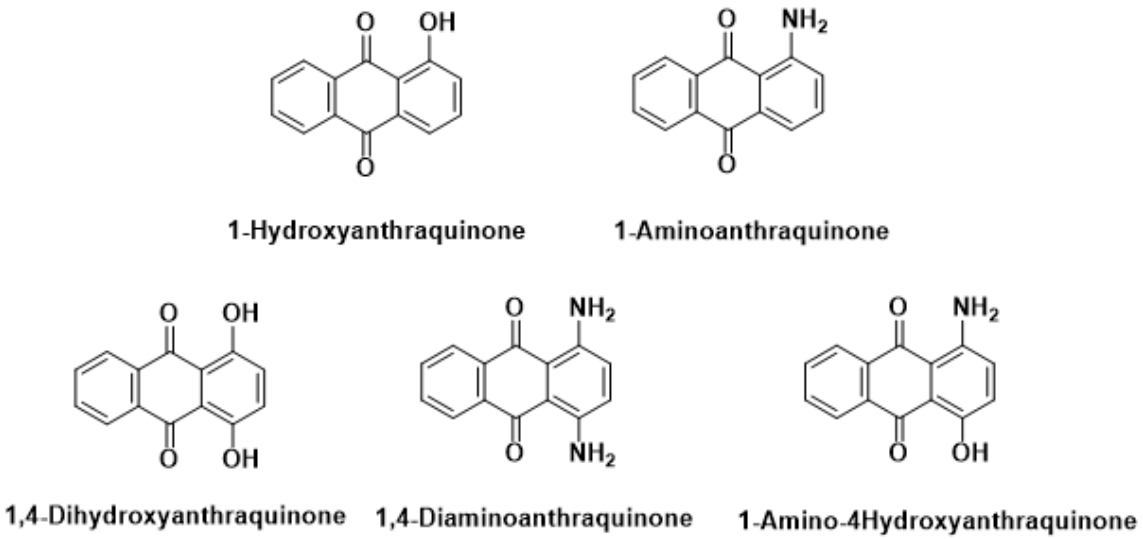

Figure 3: Used AQ derivatives.

In this internship AQs are characterized optically through Infrared spectroscopy (IR) as well as by UV-vis spectroscopy and photoluminescence spectroscopy (PL). For the electrochemical carbon dioxide capturing spectroelectrochemistry under N_2 and under CO_2 were performed.

The reason why specifically using AQs for this study, was the fact that similar cyclic voltammetry had already be carried out under N_2 and CO_2. Yin et al. as well as Shamsipur et al. proposed that under N_2 first the radical anion and then the dianion is formed [21,49].

$$Q + e^- \rightarrow Q^{\cdot -} \qquad \text{Eq. 8}$$

$$Q^{\cdot -} + e^- \rightarrow Q^{2-} \qquad \text{Eq. 9}$$

It is expected that the AQ under CO_2 behaves like the reduction of AQ under N_2 (Eq 8, Eq 9.). The difference lays in an additional step where it is proposed that the CO_2 is binding itself to the formed AQ dianion [21].

$$Q^{2-} + 2\,CO_2 \rightarrow Q(CO_2)_2^{2-} \qquad \text{Eq. 10}$$

Gurkan et al. supposed the following structure for the $Q(CO_2)_2^{2-}$ [22].

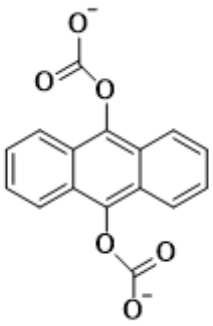

Figure 4: Possible structure of $Q(CO_2)_p^{2-}$.

For this study the process was carried out in homogenous solution, like also done by Yin et al. Through the use of different substituted AQs it is expected that the mechanism will be better understood. To gain further insights in the underlying mechanism, spectroelectrochemistry under N_2 and CO_2 in homogenous solution were carried out.

Additionally, to the before mentioned experiments and characterization methods a chronoamperometry under O_2 was performed. Here, the anthraquinones were used because they are considered as electrocatalysts for the production of H_2O_2 for decades. The chronoamperometry was performed in aqueous solution as well as in non-aqueous solution [50,51].

2. Experimental

2.1 Purification of the material

For all following experiments purified AQ's were used. The materials were purified through sublimation. All materials except the 1-Hydroxyanthraquinone as well as the 1-Aminoanthraquinone were sublimated two times by Dr. Mihai Irimia-Vladu. The before mentioned AQ's were only sublimated 1 time by Mihai and me.

For the sublimation two glass tubes were melted together. A "boat" aluminium foil was built. The material was filled into the boat which was put into the glass tube and then given into the apparatus. The apparatus was heated up. Due to the high sublimation point of the anthraquinones, a vacuum was created in order to lower this point. On the next day, the purification was finished, and the purified material could be used.

In Figure 5 the vacuum sublimation apparatus with the sublimated 1-Hydroxyanthraquinone can be seen.

Figure 5: Vacuum sublimation apparatus with 1-Hydroxyanthraquinone.

2.2 Optical characterization

2.2.1 Infrared Spectroscopy

For the optical characterization through IR spectroscopy the solid and purified AQ derivative were used. The IR measurement was performed on a Bruker VERTEX 80-ATR spectrometer in the spectral range of 4000-500 cm^{-1}, 64 scans were averaged and a resolution of 2 cm^{-1} was chosen.

2.2.2 UV-vis spectroscopy and photoluminescence spectroscopy (PL)

For the UV-vis spectroscopy a Varian Cary 3G UV-visible spectrophotometer was used. The measurement was performed in a wavelength range of 300 to 700 nm. For the measurements a 1 mM AQ derivative stock solution was diluted to 100 and 50 µM. The stock solution as well as the dilutions were prepared in acetonitrile (MeCN). Approximately 3 mL of the respective solution was used for the measurements. Special attention was paid to the resulting absorbance. If the absorbance was above 1, the solution was too concentrated and had to be further diluted.

Before the PL spectrum could be recorded a UV-vis measurement had to be carried out. Through the resulting UV-vis spectrum of the respective material the absorptions maxima were determined. The wavelength where the absorptions maximum was found is the excitation wavelength for the PL measurement.The Photoluminescence measurements of the AQ derivative solutions were carried out on a PTI QuantaMaster 40 spectrofluorometer using a dual monochromator setup on the excitation as well as the emission channel. The slit widths in the excitation channel were set to 2 mm, while 1 mm slit widths were used in the emission channel. Additionally, a 320 nm long-pass filter was placed in the excitation light path to block light from lower orders of diffraction.

For the PL spectroscopy a 2 mM AQ derivative stock solution was diluted to 1 mM, 100, 10, and 1 µM. The solution was filled into PL cuvette and put into the spectrometer. It was measured from the lowest concentration up to the highest for each molecule except the unsubstituted AQ. For each material a excitation spectrum as well as a further absorbance spectrum was measured.

2.3 Preparation of the working electrode (WE)

As WE a polished and activated glassy carbon electrode (GCE) was used. Before the GCE was used it had to be polished with different aluminium pastes to get rid of remaining films and contaminations. It was started with a particle size of 1 µm going down to 0.3 and 0.05 µm. The last polishing step was carried out with toothpaste. For polishing the GCE was moved in an 8 shape for approximately 30 s on each side. Between each polishing step the GCE was washed and sonicated with 18 MΩ water and isopropanol for 15 min. After polishing the GCE had to be activated. Therefore, cyclic voltammetry was performed by using a 0.5 M H_2SO_4 , a Ag/AgCl/3 M KCl reference electrode, and a Platinum wire as counter electrode were used . The parameters for the CV are listed in Table 1 .

Table 1: Parameters for GCE activation.

Potential range / mV	Current range / mA	Starting potential / mV	Scan rate / mV s^{-1}	Number of scans
-1000 to 1500	100	0	50	30

2.4 Preparation of the Ag/AgCl quasi-reference electrode (RE)

For the construction of the quasi-reference electrodes a Jaissle Potentiostat-Galvanostat 1030.PCT was used. As CE a platinum wire and blade were used while a Ag/AgCl/3 M NaCl was used as RE. Clean and sanded silver wires were used as WE. Before the Ag wires were used, they were grinded with abrasive paper to remove the old coating. All three electrodes were put into a beaker with 1 M HCl. The parameters for the CV are listed in Table 2.

Table 2: Parameters for the production of the quasi RE.

Potential range / mV	Scan rate / mV s^{-1}	Number of scans
-400 to 700	10	10

After the CV a potential of 300 mV was applied for 120 s. Then the electrodes were rinsed with 18 MΩ water before a potential of 700 mV was applied for 15 min.

2.5 Electrochemistry under N_2 and CO_2

For the electrochemical investigation under N_2 and CO_2 a one compartment cell consisting of a 25 mL vial covered with a cap and a septum was used. The three electrodes (WE GCE, CE Platinum wire, and RE Ag/AgCl wire) were inserted through the septum. A magnetic stirrer bar and the according amount of AQ derivative for a 2 mM were put into the vial before it was transferred into the glove box. In the glove box 10 mL of an 0.1 M acetonitrile solution with tetrabutylammonium hexafluorophosphate ($TBAPF_6$) as electrolyte salt was used. The set up of the electrochemical cell can be seen in Figure 6 .

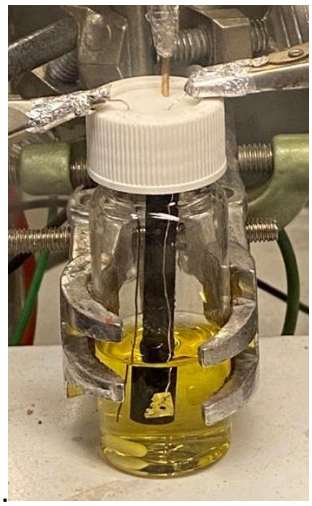

Figure 6: Electrochemical cell with GC as WE, Platinum wire as CE, and Ag/AgCl as RE.

All cyclic voltammetry (CV) curves were recorded with a Vertex One Ivium potentiostat/Galvanostat. The CVs under N_2 were taken in a potential range of -2.0 to 1.8 V

with a scan rate of 200 mV s^{-1}. Since the reductive side was of greater interest, CVs in a potential range of -2.0 to +0.5 V were recorded at different scan rates (400, 200, 100, 50, 20, and 10 mV s^{-1}).

To reach a CO_2 saturated environment the solution was bubbled with CO_2 for 15 min. The CVs under CO_2 were recorded in a potential range of -2.2 to +0.5 V with the same variation of scan rates which were used for the measurements under N_2.

For better comparison with literature the potentials were converted from "against Ag/AgCl" to "against standard hydrogen electrode (SHE)". Therefore, a Ferrocene calibration was necessary. Ferrocene was used due to its fixed and known potential against SHE (+0.64 V vs. SHE) [18]. For the calibration the Ferrocene was added to the measured solution. After stirring for some seconds a CV in the potential range of -0.5 to +1.0 V was recorded with a scan rate of 50 mV s^{-1}.

2.6 Gas Chromatography (GC)

For the detection of gaseous products (like CO) a gas injection gas chromatography was performed. Therefore, 2 mL of the gas phase were taken and inserted into a Thermo Scientific Trace GC Ultra with a Restek molecular sieve packed column and thermal conductivity detector (TCD). Sicnce the sample was investigated for CO, He as carrier gas was used.

2.7 Spectroelectrochemistry under N_2 and CO_2

For the spectro-electrochemical characterization a special 1 mm thin-layer-quartz glass cuvette from Basi was used. As WE a platinum mesh was used while as CE a Platinum wire and as RE a Ag/AgCl quasi reference electrode was used (Figure 7).

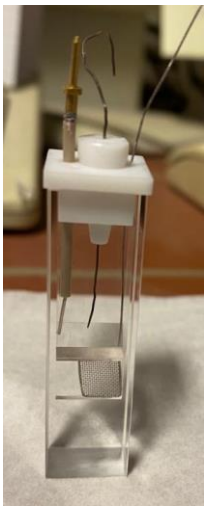

Figure 7: Spectro-electrochemical cell with Pt-mesh as WE, Pt wire as CE, and Ag/AgCl as quasi RE.

This cuvette was filled with an 1 mM AQ derivative solution which was bubbled with CO_2 for 15 min. Before the reduction and the UV-vis recording was started the whole system was bubbled with a CO_2 balloon to guarantee a CO_2 saturated environment. The electrochemical reduction was carried out with an Ivium potentiostat decreasing the potential from 0 V to -2.2 V. Therefore, every 37 s the potential decreased by 200 mV. While reducing the material electrochemically UV-vis spectra were recorded. Here, the Varian Cary 3G UV-visible spectrophotometer was used with a scan rate of 1515 nm/min. For conversion of the potential against Ag/AgCl to the potential against SHE a calibration with ferrocene was performed.

2.8 Cyclic voltammetry (CV)

Of each material in non-aqueous solution a cyclic voltammetry (CV) was performed. Therefore, a one compartment cell (Figure 6) was used. A platinum wire was used as CE and a GCE was used as WE. As RE the before produced Ag/AgCl quasi-reference electrodes were used. The CVs were recorded with a scan rate of 50 mV s^{-1} in a potential range of 500 to -2200 mV under N_2 and O_2.

For the CVs in aqueous solution two-compartment cell was used. The two sides are separated with a Nafion N-117 membrane (0.180 mm thick, ≥ 0.90 meq/g exchange capacity). On the one side a platinum wire was used as counter electrode (CE). On the other side a Ag/AgCl/3 M KCl reference electrode and a GCE as working electrode were used. In both sides a magnetic stirrer bar was placed. The CVs were recorded with a scan rate of 50 mV s^{-1} in a potential range of 0 to -1500 mV under N_2 and O_2.

2.9 Chronoamperometry in aqueous solution

The chronoamperometry was performed in a two-compartment cell with a platinum CE, GCE WE, and a Ag/AgCl/3 M KCl RE. Both sides were equipped with an magnetic stirrer bar. On the counter side the cell was filled for each experiment with 0.1 M NaOH. The liquid on the working side was chosen accordingly to the performed experiment. It was important that the GCE was immersed 1 cm for each experiment. Before the chronoamperometry was started the electrolyte was purged with N_2 for 40 min and then with O_2 for 30 min to ensure a oxygen saturated system. To guarantee a O_2 saturated environment during the chronoamperometry the head space was bubbled with O_2. The chronoamperometry was recorded for 6 h at a potential of -400 mV vs. SHE. After 0, 1, 2, 4, and 6 h a 150 µL aliquot was taken from the working electrode side for the H_2O_2 determination.

2.10 Chronoamperometry in non-aqueous solution

The chronoamperometry in non aqueous solution was performed in a one compartment cell. As CE a platinum wire, as WE a GCE, and as WE a Ag/AgCl quasi-reference electrode was used. The electrolysis of the 2 mM AQ derivative solution in MeCN was carried out at -1100 mV vs.

Ag/AgCl quasi RE for 2 h. In contrast to the chronoamperometry in aqueous solution the head space was not bubbled with O_2 due to the evaporation of the solvent. After 0, 30, 60, 90, and 120 min a 150 µL aliquot of the solution was taken for the H_2O_2 determination.

2.11 H_2O_2 determination

For the determination and quantification of H_2O_2 UV-vis spectroscopy was used. Therefore, the method established by Apaydin et al. at our institute was used [18,52,53].

Generally, it known that *p*-Nitrobenzeneboronic acid (*p*-NPBA) reacts with hydrogen peroxide in an alkaline solution to a p-nitrophenolate [54]. The reaction scheme is shown in Figure 8 .

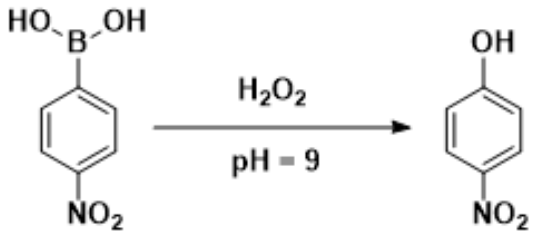

Figure 8: General reaction scheme of the reaction of p-NPBA with H_2O_2 in alkaline solution.

The boronic compound has an absorbance maximum of around 294 nm in a carbonate/bicarbonate buffer system (pH 9) while the phenol derivative has a maximum at around 405 nm [54].

For the calibration curves standard solutions containing an amount of 1, 2, 4, 10, 20, 80, and 160 nmol H_2O_2 were prepared. A 4 mM p-NPBA solution was manufactured and mixed in 1:1 ratio with a 150 mM carbonate buffer (pH 9). This mixture was filtered with a PES 0.45 µm syringe filter. To 50 µL of the respective standard solution 2 mL of the filtered mixture were added. After a reaction time of 36 min 100 µL were used for the recording of the UV-vis spectra. The UV-vis measurements were caried out with a Thermo Scientific Multiscan Go spectrometer. The calibration curves for H_2O_2 in aqueous solution as well as for H_2O_2 in MeCN solution can be seen in Figure 9 and 10.

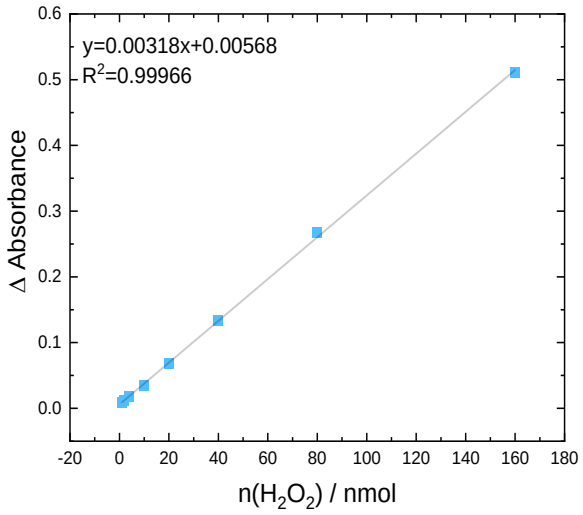

Figure 9: Calibration in aqueous solution.

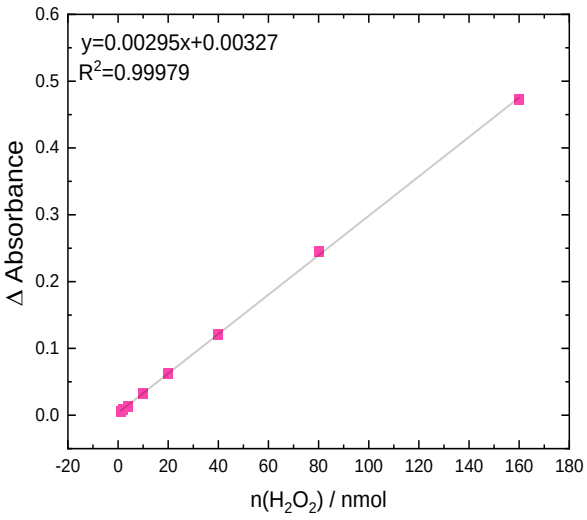

Figure 10: Calibration in MeCN.

In the Figures above the linear behaviour between the absorbance and the produced amount of H_2O_2 can be clearly seen. Both calibration lines have an intercept d of approximately 0. Furthermore, it can be seen that the slope of both curves is nearly the same. The slope in aqueous solution is steeper than in MeCN.

3. Results and Discussion

3.1 IR spectroscopy

The solid purified AQ derivatives were measured, and the results plotted in a wavenumber range of 4000 to 500 cm^{-1}. The resulting spectra are shown in Figure 11 - 16.

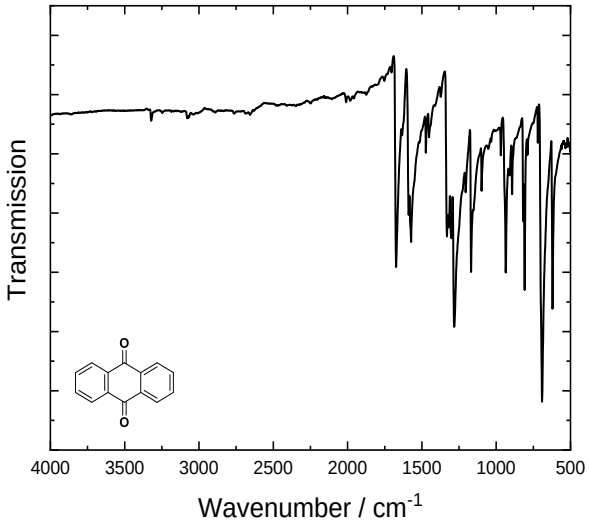

Figure 11: IR spectrum of AQ.

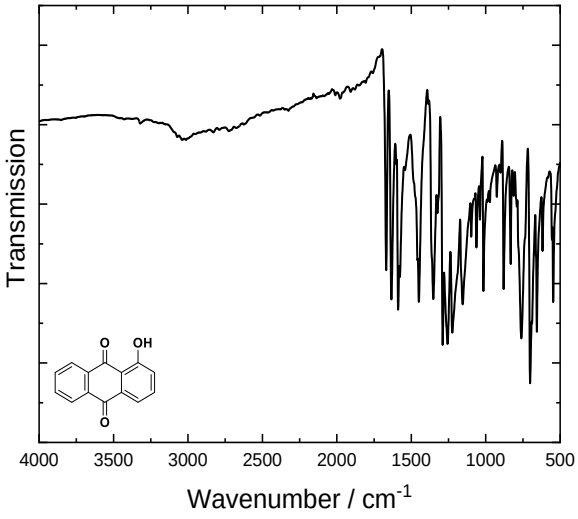

Figure 12: IR spectrum of 1-Hydroxyanthraquinone.

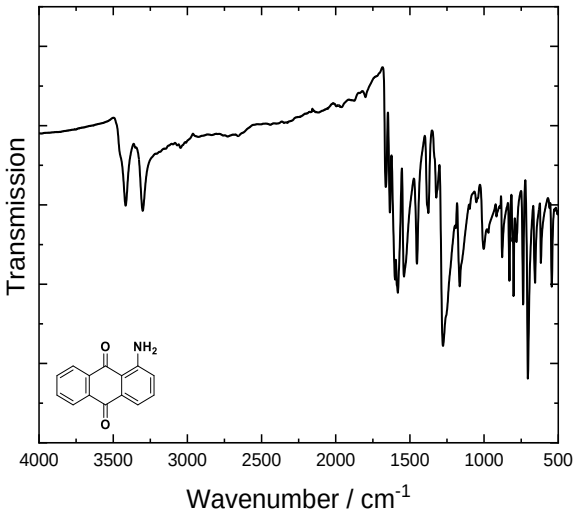

Figure 13: IR spectrum of 1-Aminoanthraquinone.

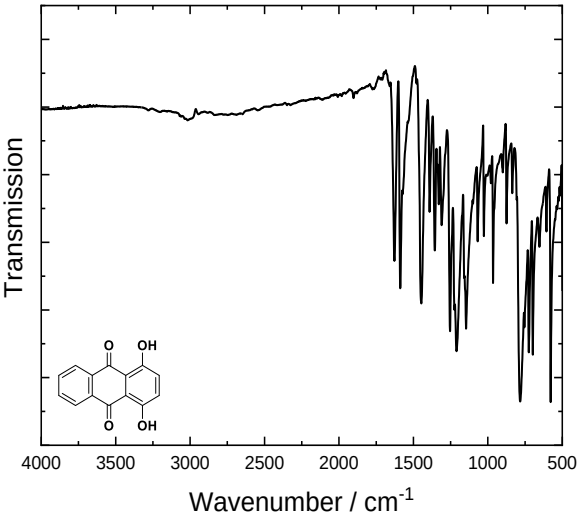

Figure 14: IR spectrum of 1,4-Dihydroxyanthraquinone.

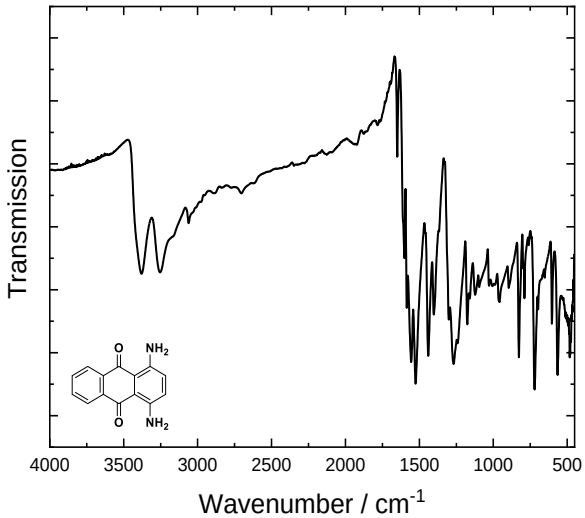

Figure 15: IR spectrum of 1,4-Diaminoanthraquinone.

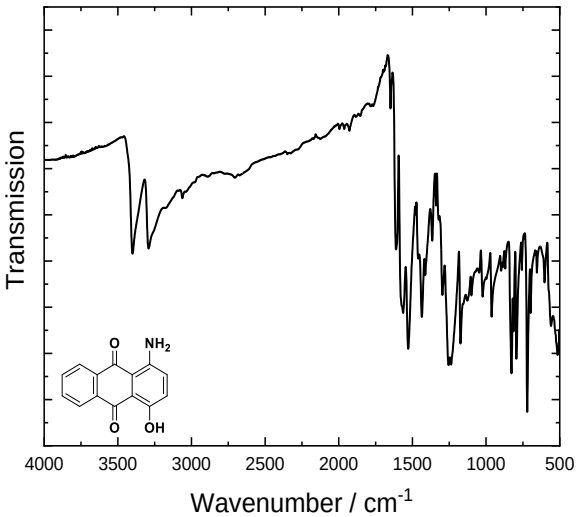

Figure 16: IR spectrum of 1-Amino-4-hydroxyanthraquinone.

Generally, an IR spectrum provides information about the molecules IR absorbance. Functional groups remain on the same range independent of the molecules structure . For the used AQ derivatives the following ranges are important: 3300-3500 cm^{-1} (Amino groups), 3000-3200 cm^{-1} (Hydroxy groups), and 1600-1800 cm^{-1} (Carbonyl group) [55,56,57]. The exact values for each molecule are listed in Table 3.

Table 3: Position of carbonyl, amino, and hydroxy groups.

Material	Carbonyl group	Amino group	Hydroxy group
Anthraquinone	1674	-	-
1-Hydroxyanthraquinone	1633, 1670	-	3033
1-Aminoanthraquinone	1635, 1662	3304, 3416	-
1,4-Dihydroxyanthraquinone	1628	-	3018
1,4-Diaminoanthraquinone	1650	3253, 3381	-
1-Amino-4-hydroxyanthraquinone	1612, 1649	3294, 3340	3061

It is noticeable that the symmetric AQ derivatives (AQ, 1,4-Dihydroxyanthraquinone, and 1,4-Daminoanthraquinone) show one carbonyl peak while the asymmetric molecules (1-Hydroxyanthraquinone, 1-Aminoanthraquinone, and 1-Amino-4-hydroxyanthraquinone) show two carbonyl peaks. The amino group peaks are sharp peaks and clearly visible in the respective plots while the hydroxy group peaks are broader and less resolved.

3.2 UV-vis and PL spectroscopy

In Figure 17a all AQ derivatives are shown. In 17b the 1,4-Dihydroxyanthraquinone, the 1-Aminoanthraquinone, the 1,4-Diaminoanthraquinone, and the 1-Amino-4-hydroxyanthraquinone under a UV lamp are shown.

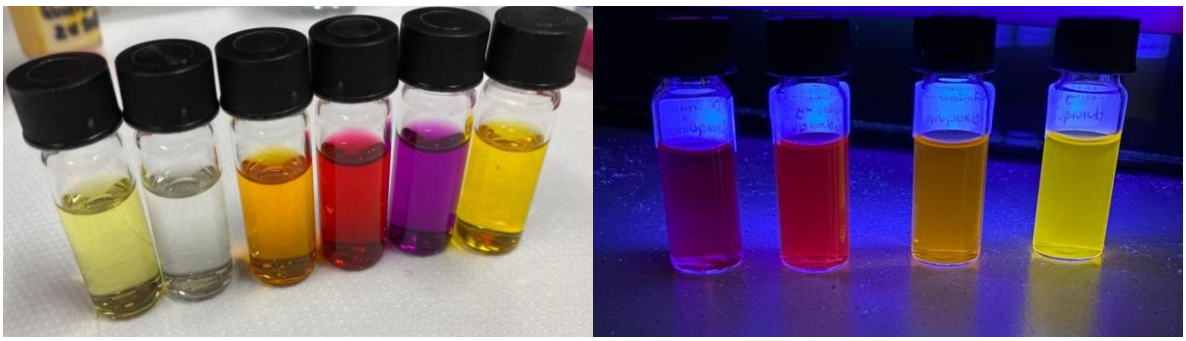

Figure 17a: Anthraquinone derivatives in normal light. b: AQ derivatives under UV lamp with a wavelength of 365 nm.

The absorbance as well as the PL spectra are shown in Figure 18 - 22.

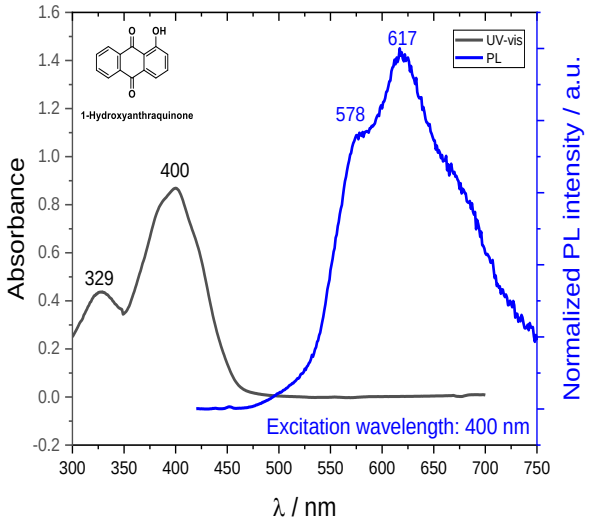

Figure 18: UV-vis and PL spectrum of 1-Hydroxyanthraquinone.

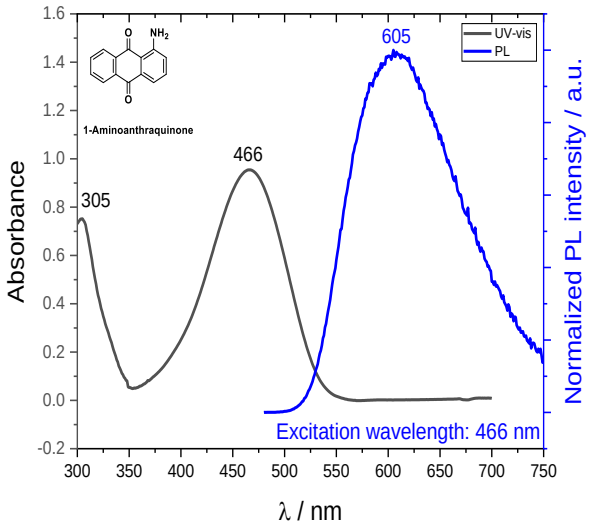

Figure 19: UV-vis and PL spectrum of 1-Aminoanthraquinone.

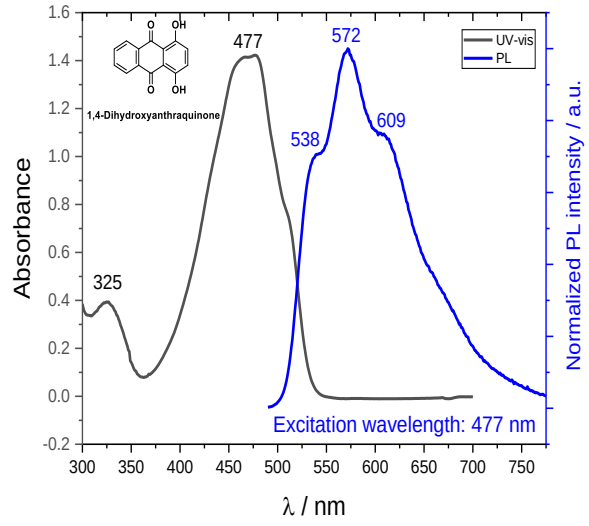

Figure 20: UV-vis and PL spectrum of 1,4-Dihydroxyanthraquinone.

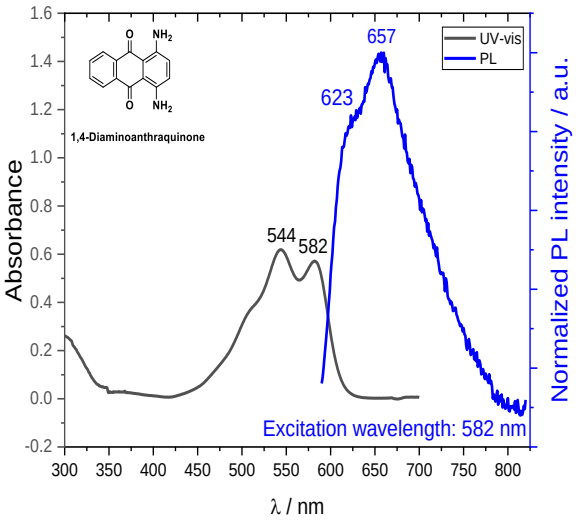

Figure 21: UV-vis and PL spectrum of 1,4-Diaminoanthraquinone.

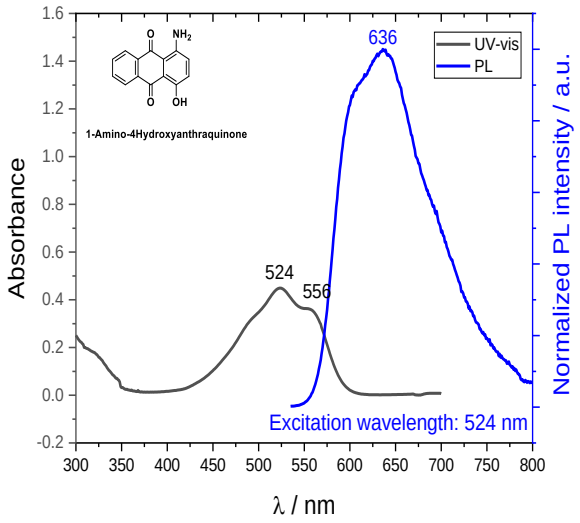

Figure 22: UV-vis and PL spectrum of 1-Amino-4-hydroxyanthraquinone.

The different emissions spectra show different shapes. So, the amino substituted AQs have one or two peaks in the emissions spectra while the hydroxy substituted AQs have two or thee peaks. A reason for the "shape" of the emissions peaks can be tautomers or a hydrogen binding [58,59].

For all molecules the stoke shift was calculated. Therefore, the wavelength of the emission and absorbance maximum was considered. The absorbance and emission maximum as well as the stoke shift are listed in Table 4.

Table 4: Absorbance maxima of UV-vis and PL spectrum, and calculated Stoke Shift.

Material	λ_{Abs} max in eV (UV-vis)	λ_{Em} max in eV (PL)	Stoke shift in eV
Anthraquinone	3.90	-	-
1-Hydroxyanthraquinone	3.10	2.01	1.09
1-Aminoanthraquinone	2.60	2.17	0.43
1,4-Dihydroxyanthraquinone	2.66	2.05	0.61
1,4-Diaminoanthraquinone	2.13	1.89	0.24
1-Amino-4-hydroxyanthraquinone	2.37	1.95	0.42

In Table 4 it gets visible that the stoke shift for the 1-Hydoxy-AQ is bigger than for all others. Basically, all used AQ derivatives with at least one hydroxy group show a bigger stoke shift than AQ derivatives with a amino group.

3.3 Electrochemistry under N_2

In Figure 23 the CV curves from all materials in a potential range of -2.0 to +1.8 V are shown. The CVs were recorded with a scan rate of 200 mV s^{-1}.

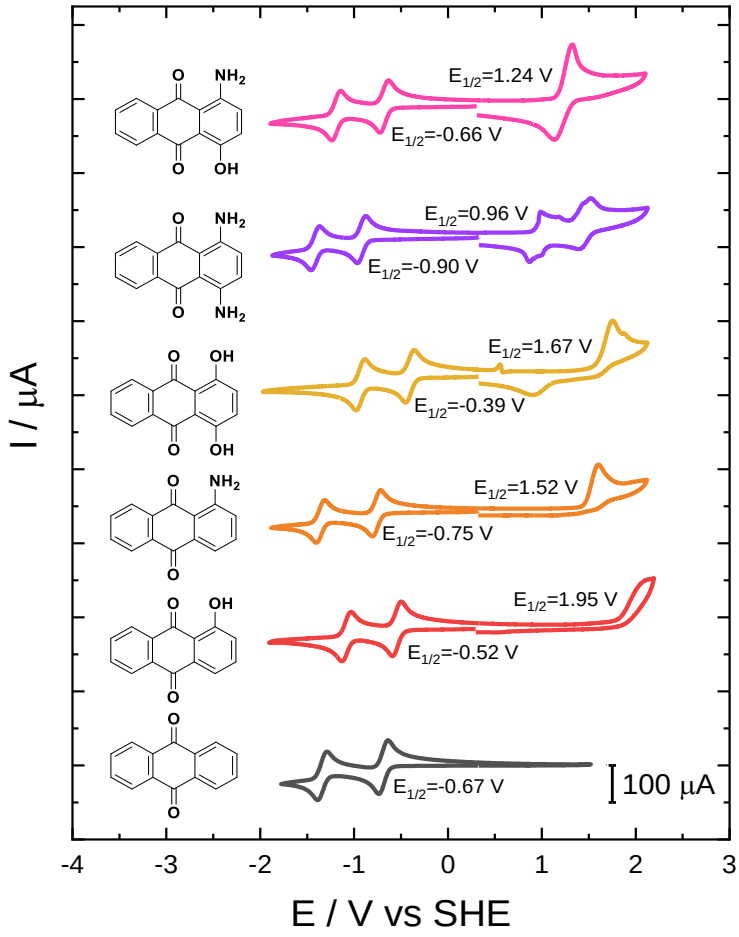

Figure 23: Full CV scans under N_2 showing oxidation and reduction of all 6 materials.

Figure 23 shows for each material except the unsubstituted AQ at least one oxidation peak. For the anthraquinone a detection of an oxidation peak was not possible due to the fact that the potential is too far in the anodic regime for this electrochemical setup. An irreversible oxidation was detected for the 1-Aminoanthraquinone and the 1-Hydroxyanthraquinone. For the 1,4-Diaminoanthraquinone and the 1-Amino-4-hydroxyanthraquinone the oxidation is reversible.

Furthermore, in the Figure above it can be seen that each material shows two reversible one electron reduction steps. This proves that the reduction of AQ and also its derivatives is a two-step mechanism, as it was mentioned in chapter 1.4 . For comparison the half-step potential of the first reduction step was calculated for each material. The potential of the unsubstituted AQ ($E_{1/2}$) was chosen as reference point. Upon comparison the influence of the different substituents can be observed. Due to the electron withdrawing properties of both groups a shift in the same direction was expected [60]. However, the measurement showed that the amino groups shift the potentials cathodically while the hydroxy groups shift the potential anodically [49,60]. The potential of the 1-Amino-4-hydroxyanthraquinone is nearly the same as the unsubstituted AQ. To highlight the difference in location of the reduction peaks, a table with the half-step potentials is provided.

Table 5: Half step potentials of the materials.

Material	***1st reduction peak***	***2nd reduction peak***
Anthraquinone	*-0.67 V*	*-1.32 V*
1-Hydroxyanthraquinone	*-0.52 V*	*-1.06 V*
1-Aminoanthraquinone	*-0.75 V*	*-1.34 V*
1,4-Dihydroxyanthraquinone	*-0.39 V*	*-0.91 V*
1,4-Diaminoanthraquinone	*-0.90 V*	*-1.39 V*
1-Amino-4-hydroxyanthraquinone	*-0.66 V*	*-1.17 V*

Furthermore, for all materials except the unsubstituted AQ the HOMO-LUMO was calculated. Therefore, the onset of the first reduction peak as well as from the first oxidation peak under N_2 were used. The values were converted in eV and then compared to the optical HOMO-LUMO from the UV-vis measurements. The results are listed in Table 6.

Table 6: Calculated HOMO-LUMO from CV onset and compared to the optical HOMO-LUMO transition.

Substance	**HOMO-LUMO (calculated from CV in eV)**	**λ / nm**	**HOMO-LUMO (from UV-vis in eV)**
Anthraquinone	-	322	3.85
1-Hydroxyanthraquinone	2.20	400	3.10
1-Aminoanthraquinone	2.09	466	2.66
1,4-Dihydroxyanthraquinone	1.79	477	2.60
1,4-Diaminoanthraquinone	1.74	582	2.13
1-Amino-4-hydroxyanthraquinone	1.71	524	2.37

In Table 6 it can be seen that the optical HOMO-LUMO is larger than those calculated from the electrochemical investigation.

3.4 Electrochemistry under CO_2

To record the CVs under CO_2 a potential range of -2.2 to +0.5 V vs. QRE and a scan rate of 100 mV s^{-1} were used (Figure 24-29).

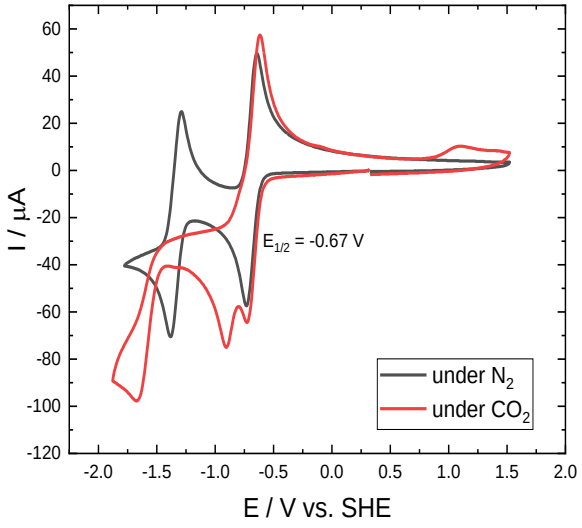

Figure 24: Anthraquinone in MeCN solution.

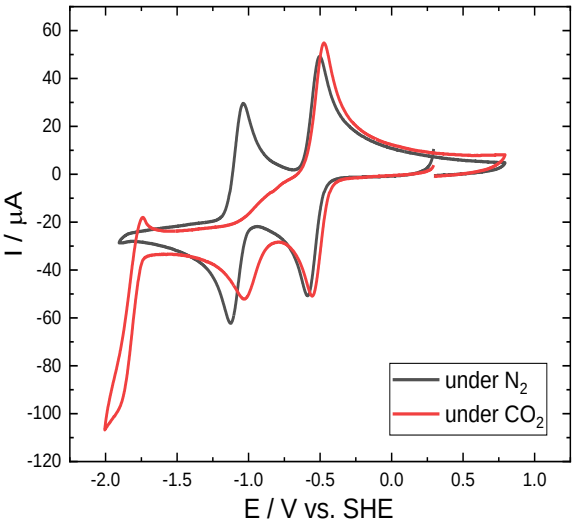

Figure 25: 1-HYdroxyanthraquinone in MeCN solution.

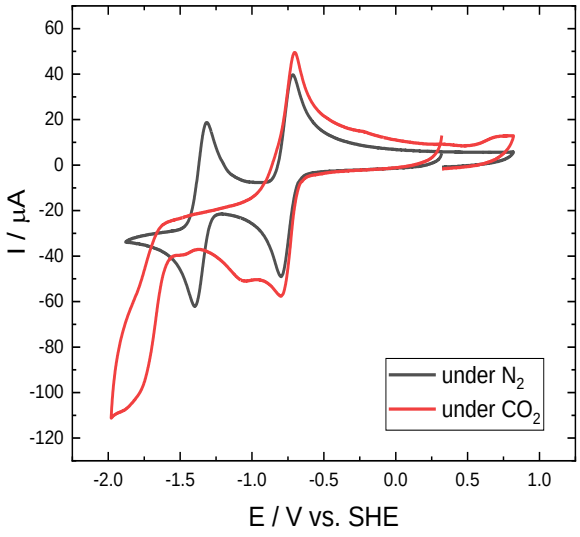

Figure 26: 1-Aminoanthraquinone in MeCN solution.

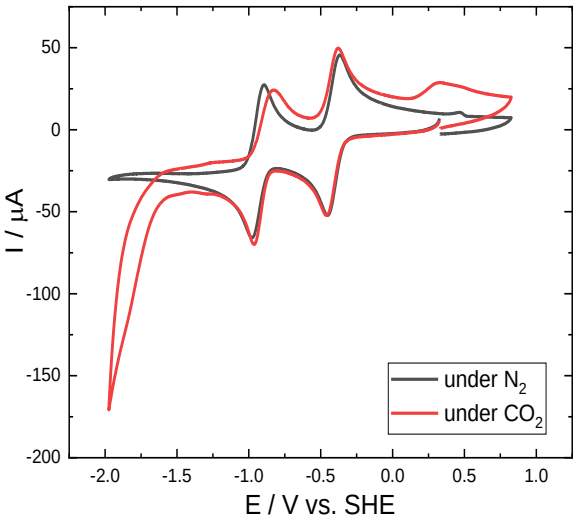

Figure 27: 1,4-Dihydroxyanthraquinone in MeCN solution.

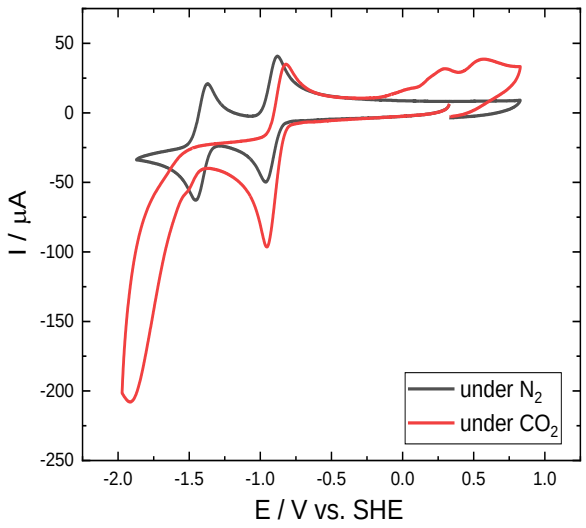

Figure 28: 1,4-Diaminoanthraquinone in MeCN solution.

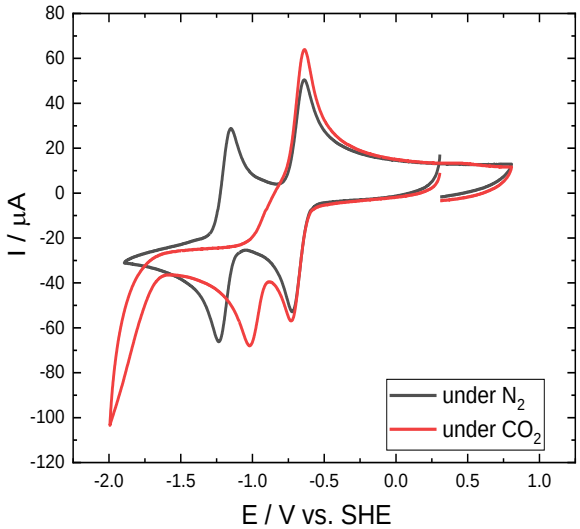

Figure 29: 1-Amino-4-hydroxyanthraquinone in MeCN.

The CVs under N_2 and CO_2 were compared they look completely different except the 1,4-Dihydroxyanthraquinone which does not show any significant differences. The half step potentials were also determined and listed in Table 7.

Table 7: Half step potential of all materials under CO_2.

Material	1st reduction peak	2nd reduction peak	3rd reduction peak
Anthraquinone	-0.66 V	-0.86 V	-1.50 V
1-Hydroxyanthraquinone	-0.49 V	-0.94 V	-
1-Aminoanthraquinone	-0.73 V	-	-1.64 V
1,4-Dihydroxyanthraquinone	-0.40 V	-0.90 V	-
1,4-Diaminoanthraquinone	-0.89 V	-	-1.47 V
1-Amino-4-hydroxyanthraquinone	-0.67 V	-0.96 V	-

In comparison to the values under N_2 it can be seen that the second reduction peak is anodically shifted while the first reduction peak remains on the same potential as under N_2 (±0.02 V). It is also noticeable that all materials except the 1,4-Dihydroxyanthraquinone show only one merged re-oxidation peak. This has been proven by integrating the curves and by comparison of the resulting charge values.

Furthermore, all materials have a high cathodic current in the potential range between -1.5 and -2.2 V. If a closer look was taken to this current a third peak in the cathodic regime can be observed for the unsubstituted AQ, the 1-Aminoanthraquinone, as well as for the 1,4-Diaminoanthraquinone. The two amino substituted AQs are also those in which the second reduction peak has been anodically shifted so strongly that the reduction peaks have merged. A reason for the strong shift could be the substituent dependent interaction of AQ derivative with CO_2. Due to the less cathodic potential which has to be used to reduce the 1-Aminoaqnthraquinone, the 1,4-Diaminoanthraquinone, as well as the unsubstituted anthraquinone to the dianion under CO_2 it is suggested that these materials get more reactive in CO_2 saturated solutions [21].

If all CVs under CO_2 are considered, it is noticeable that in a potential range of -1.5 to -2.2 V a high cathodic current is appearing. To determine whether this high current is due to the reduction of CO_2, an interaction between AQ and CO_2, or due to the fact that the potential levels were too cathodic, further experiments were carried out. The high cathodic current appears in an AQ derivative solution as well as in pure MeCN. Through this it was confirmed that the high cathodic current is caused by the WE because the potential window was exceeded. To prove the stability of the system over a longer period, 20 cycles of each material in MeCN were recorded with a scan rate of 100 mV s^{-1}. Before the experiment was started the system was bubbled with CO_2 for 15 min. The CVs of the different materials are shown in Figure 30 to 35.

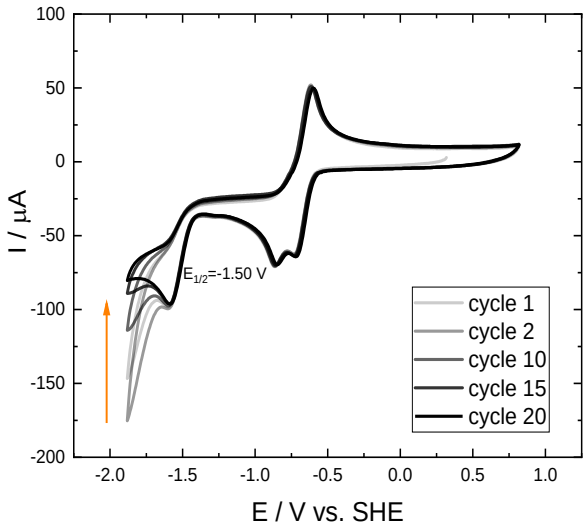

Figure 30: Cycle stability of Anthraquinone.

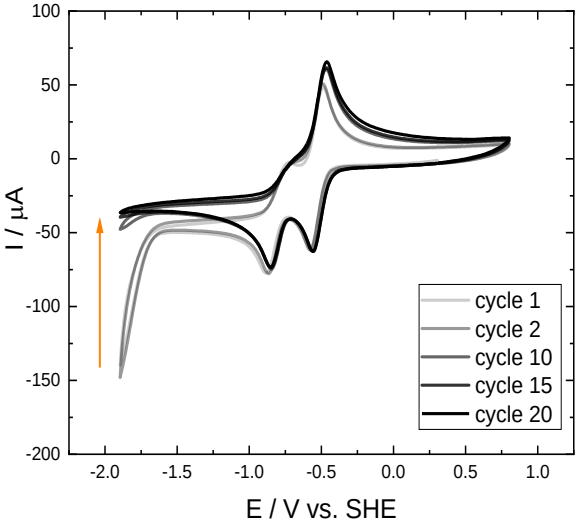

Figure 31:Cycle stability of 1-Hydroxynthraquinone.

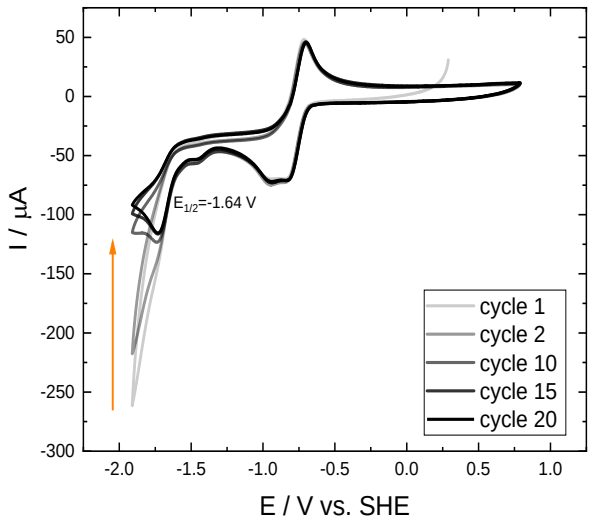

Figure 32: Cycle stability of 1-Aminoanthraquinone.

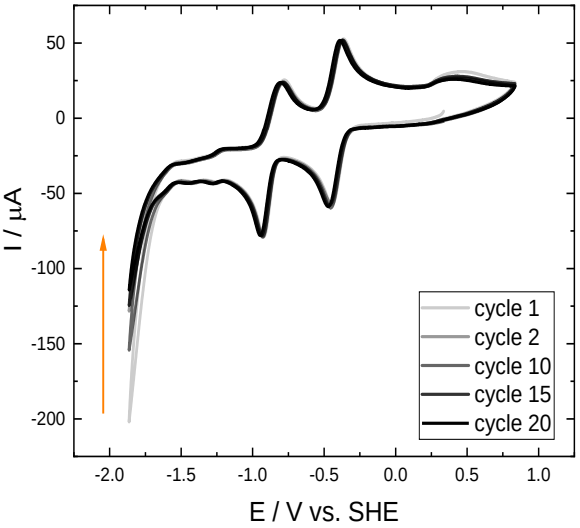

Figure 33: Cycle stability of 1,4-Dihydroxyanthraquinone.

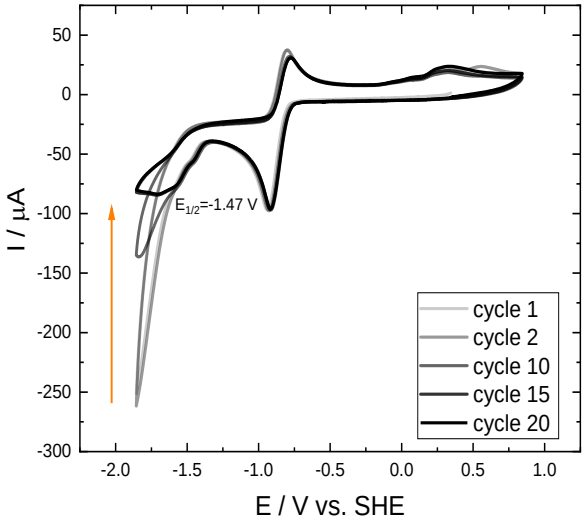

Figure 34:Figure 32: Cycle stability of 1,4-Diaminoanthraquinone.

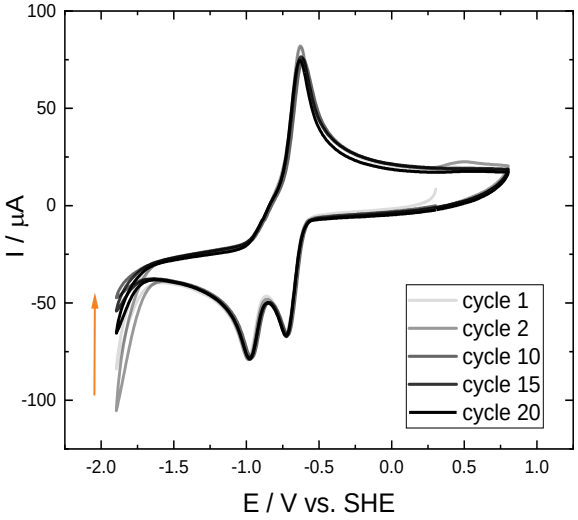

Figure 35: Figure 32: Cycle stability of 1-Amino-4-hydroxyanthraquinone.

In each Figure it can be seen that the high cathodic current decrease from cycle 1 to 20. In the case of AQ, 1-Aminoanthraquinone, as well as 1,4-Diaminoanthraquinone a smaller stable peak appeared. In the cases of AQs which are substituted with at least one hydroxy group the high cathodic current dissapeared completely. From this it can be concluded that some AQ derivatives are reacting with the CO_2. This is noticeable through an additional peak in the cathodic range (-1.45 to -1.7 V). Furthermore, this is again a hint that the cathodic current is not caused by CO_2 reduction.

In order to determine if a reduction of CO_2 is occurring a chronoamperometry under N_2 and CO_2 is performed at a potential of -1.915 V vs. Ag/AgCl quasi RE for 30 min. In the first 10 min the chronoamperometry was performed without stirring while the last 20 min the solution was stirred vigorously. In Figure 36 the current vs. time plot of the chronoamperometry of a 2 mM AQ solution in MeCN is shown.

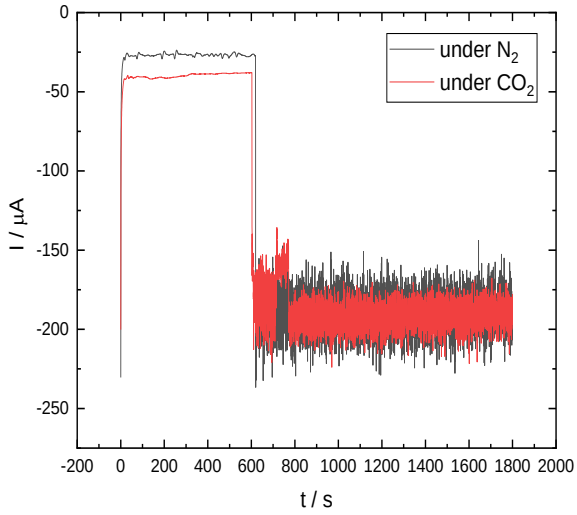

Figure 36: Chronoamperometry of an AQ solution under N_2 and CO_2.

In Figure 36 it can be seen that in the first 10 min under CO_2 a higher cathodic current was recorded. If the solution was stirred the current was equal under N_2 and CO_2. After the chronoamperometry 2 mL sample of the head space were taken. To analyse the gaseous product a gas chromatography was performed. The assumption that AQ does not reduce CO_2 was confirmed by the GC analysis, as no CO was detected.

Since there is only one reoxidation peak under CO_2 for all materials except the 1,4-Dihydroxyanthraquinone a stepwise reduction was performed according to Yin et al. [21]. The stepwise reduction of the unsubstituted AQ is shown in Figure 37.

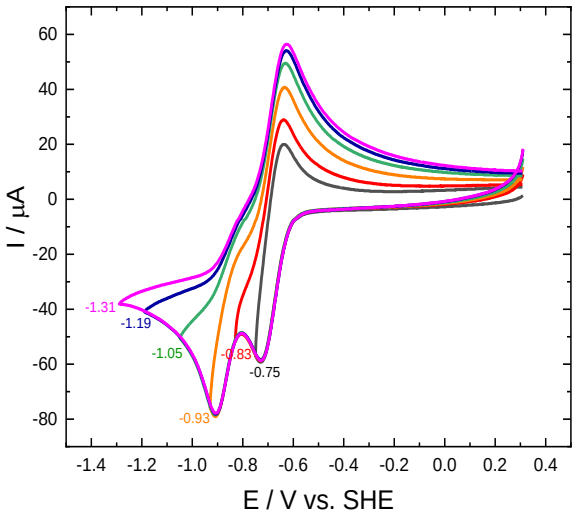

Figure 37: Stepwise reduction of AQ.

3.5 Spectro electrochemistry under N_2 and CO_2

The spectro electrochemical investigation was made in order to possibly get information about the reaction between the AQ derivative and CO_2. The relevant lines of the delta absorbance spectra under N_2 and CO_2 are shown in Figure 38-43. The UV-vis absorbance spectra under N_2 as well as under CO_2 can be found in the Appendix (chapter 5).

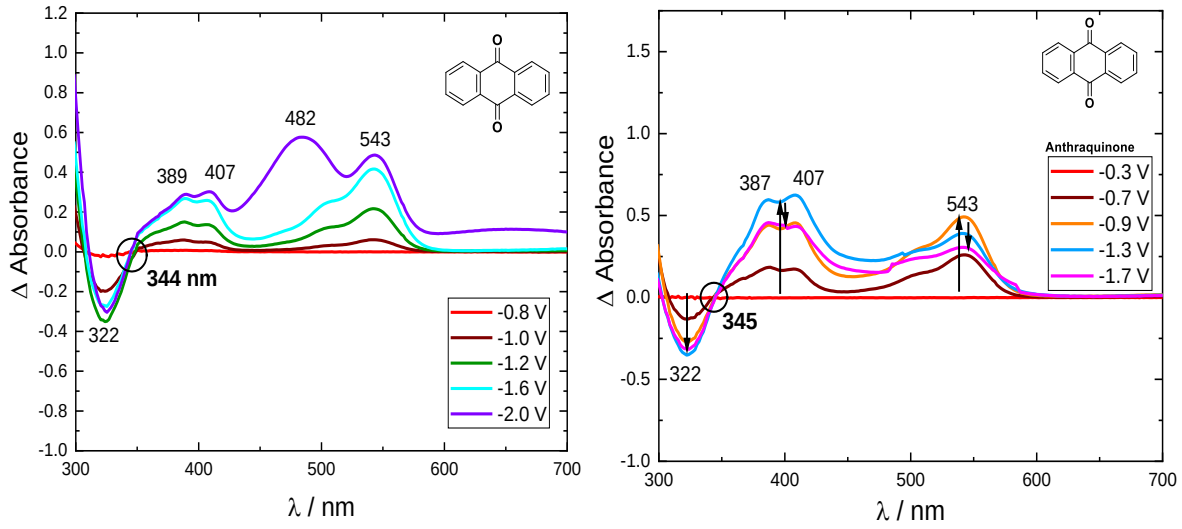

Figure 38a) Delta absorbance spectra of AQ under N_2. b) Delta absorbance spectra of AQ under CO_2.

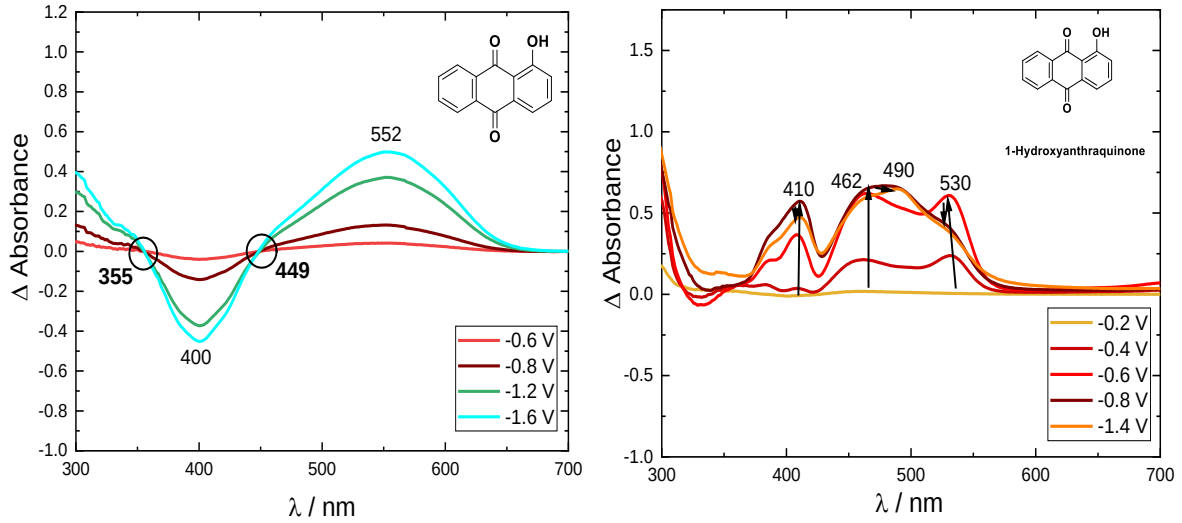

Figure 39a) Delta absorbance spectra of 1-Hydroxyanthraquinone under N_2. b) Delta absorbance spectra of 1-Hydroxyanthraquinone under CO_2.

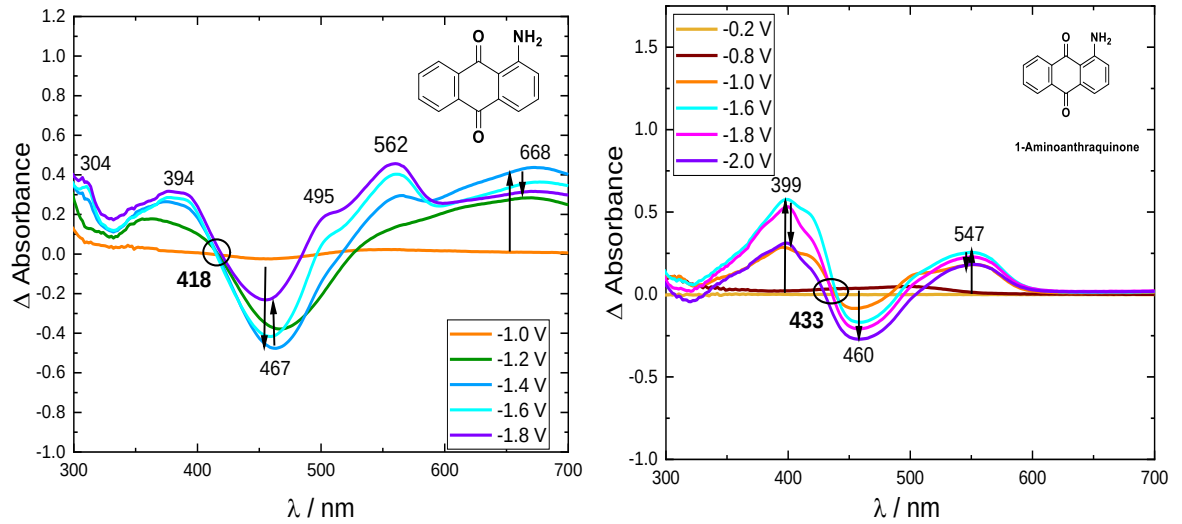

Figure 40a) Delta absorbance spectra of 1-Aminoanthraquinone under N_2. b) Delta absorbance spectra of 1-Aminoanthraquinone under CO_2.

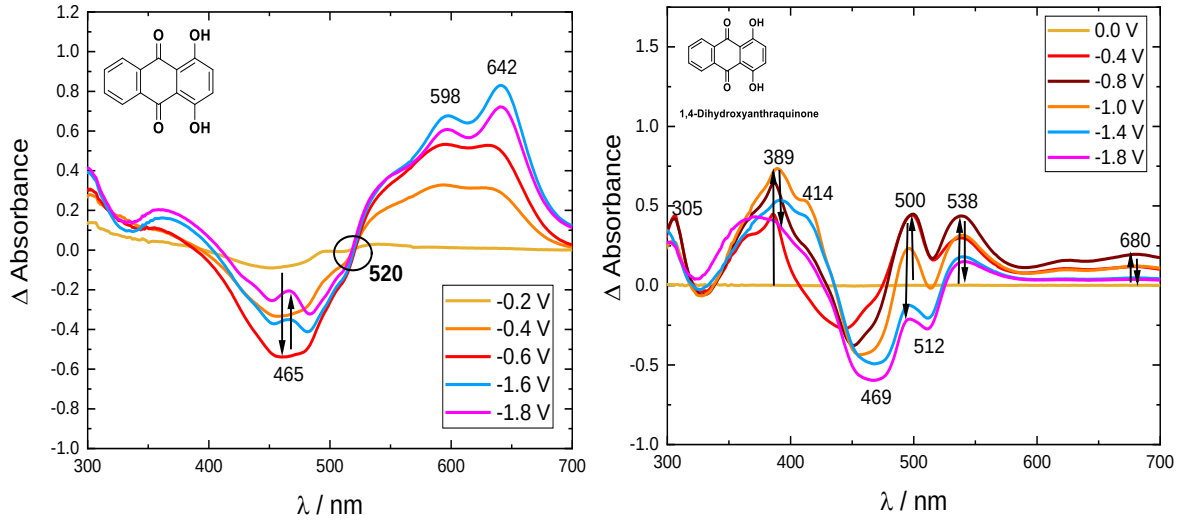

Figure 41a) Delta absorbance spectra of 1,4-Dihydroxyanthraquinone under N_2. b) Delta absorbance spectra of 1,4-Dihydroxyanthraquinone under CO_2.

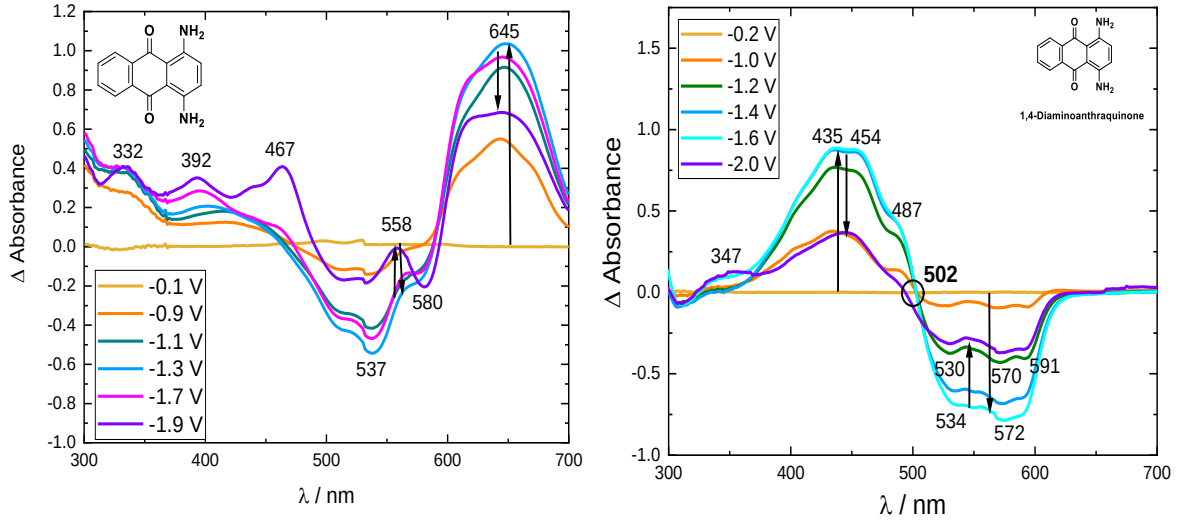

Figure 42a) Delta absorbance spectra of 1,4-Diaminoanthraquinone under N_2. b) Delta absorbance spectra of 1,4-Diaminoanthraquinone under CO_2.

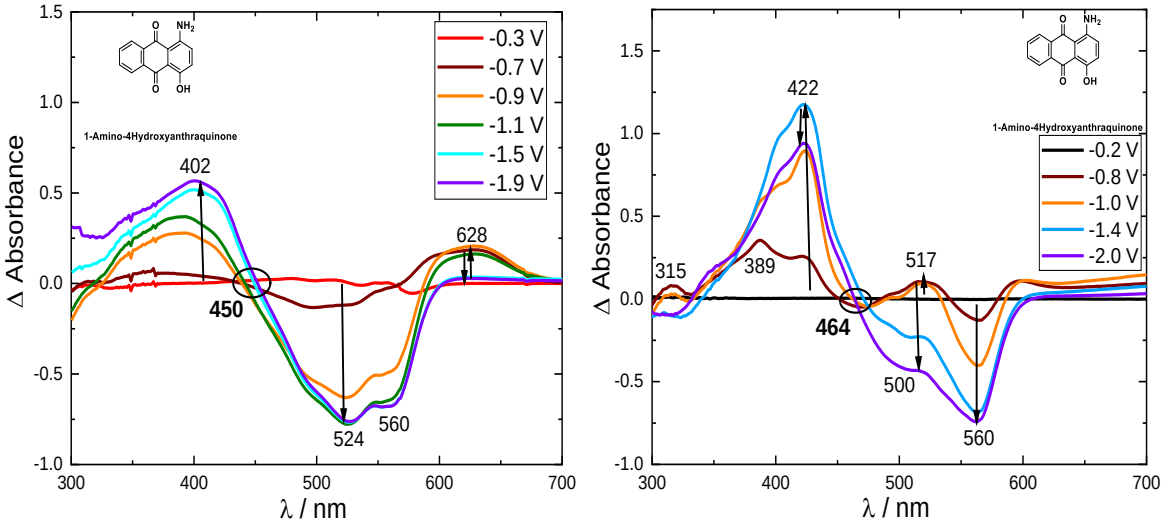

Figure 43a) Delta absorbance spectra of 1-Amino-4-hydroxyanthraquinone under N_2. b) Delta absorbance spectra of 1-Amino-4-hydroxyanthraquinone under CO_2.

If the spectra are compared under N_2 and CO_2 it is clearly visible that under CO_2 new peaks are appearing or peaks are shifted. Under N_2 a clear band at the low frequency range (around 600 nm) is visible for all materials. It is suggested that this band belongs to the first one electron reduction [61]. Furthermore, this band is only noticeable for the 1,4-Dihydroxyanthraquinone under CO_2. For the unsubstituted anthraquinone and the amino substituted anthraquinones this band above 600 nm is not visible any more in the spectra recorded under CO_2. Since the CVs of the mentioned molecules under CO_2 show also two clearly one electron reduction steps this matches with the corresponding UV-vis spectra and the appearing band in the range of 600 nm. For the molecules where in the CV under CO_2 the reduction steps are merged the band at the low frequency range is not existing.

Furthermore, at least one isosbestic point is clearly and precisely seen in the spectra under N_2 except in the spectra of the 1,4-Diaminoanthraquinone. In the spectra under CO_2 no clear and precise isosbestic point can be seen in the spectra of the pure hydroxy substituted AQs. Nevertheless, in the case of 1,4-Dihydroxyanthraquinone an appearing and a disappearing of the individual bands can be observed. In the case of 1-Hydroxyanthraquinone all bands are increasing during the reduction process, which is still not fully understood why no decreasing bands are observed.

The following Figures (44-49) show the change in absorbance in dependence of the potential under N_2 and CO_2.

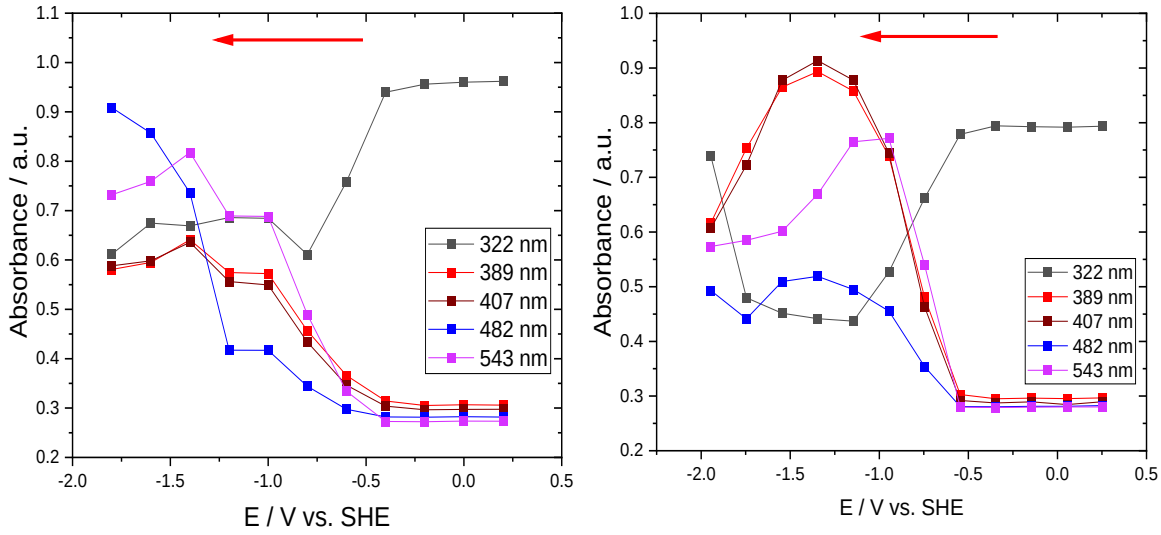

Figure 44: Absorbance vs. Potential plots at corresponding wavelength given of an AQ solution a) under N2 conditions. b) under CO2 conditions.

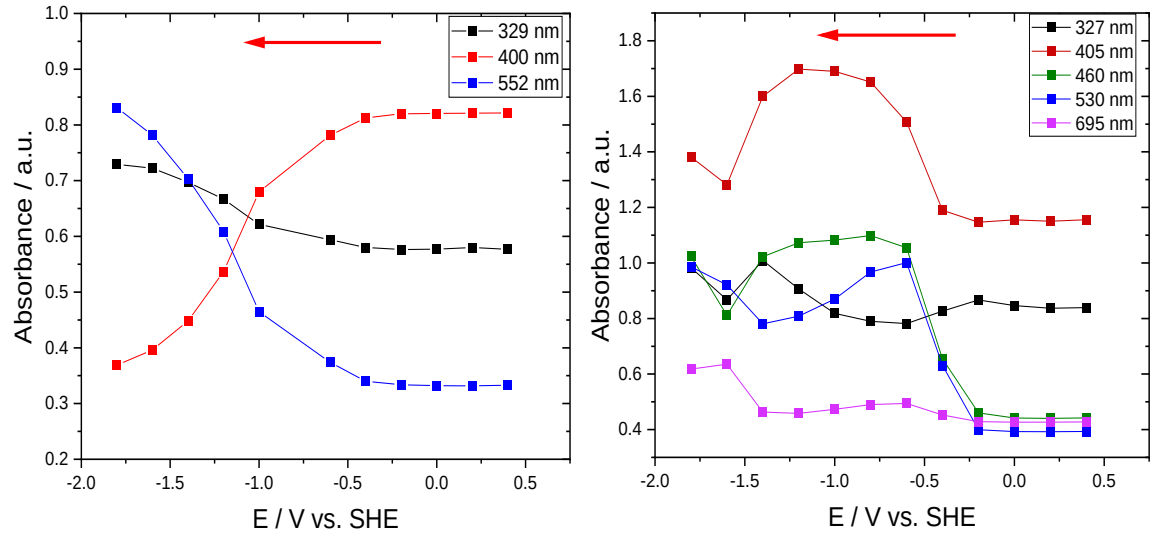

Figure 45: Absorbance vs. Potential plots at corresponding wavelength given of a 1-Hydroxyanthraquinone solution a) under N2 conditions. b) under CO2 conditions.

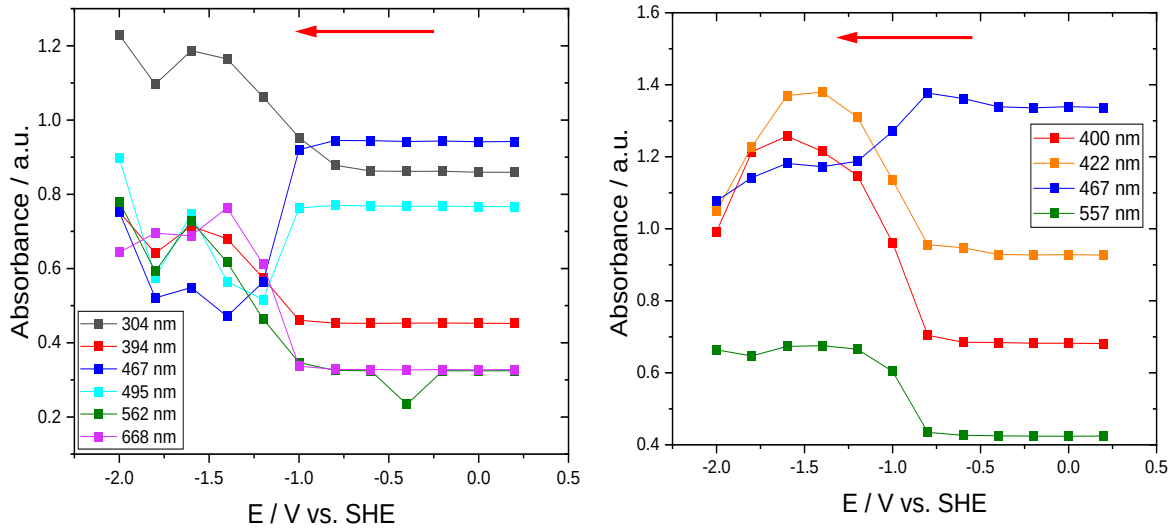

Figure 46: Absorbance vs. Potential plots at corresponding wavelength given of 1-Aminoanthraquinone solution a) under N2 conditions. b) under CO2 conditions.

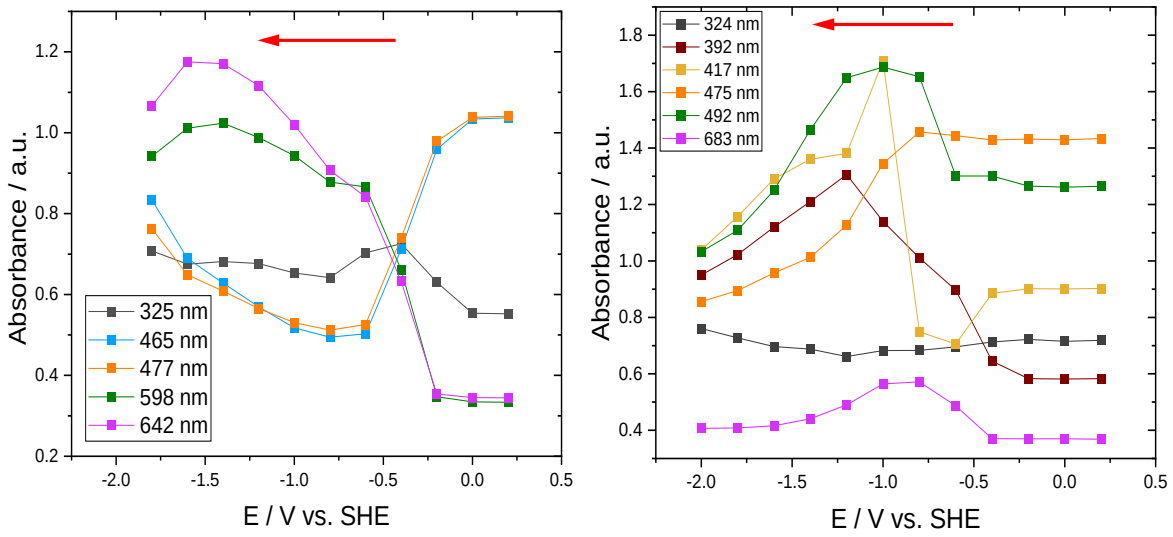

Figure 47 Absorbance vs. Potential plots at corresponding wavelength given of 1,4-Dihydroxyanthraquinone solution a) under N2 conditions. b) under CO2 conditions.

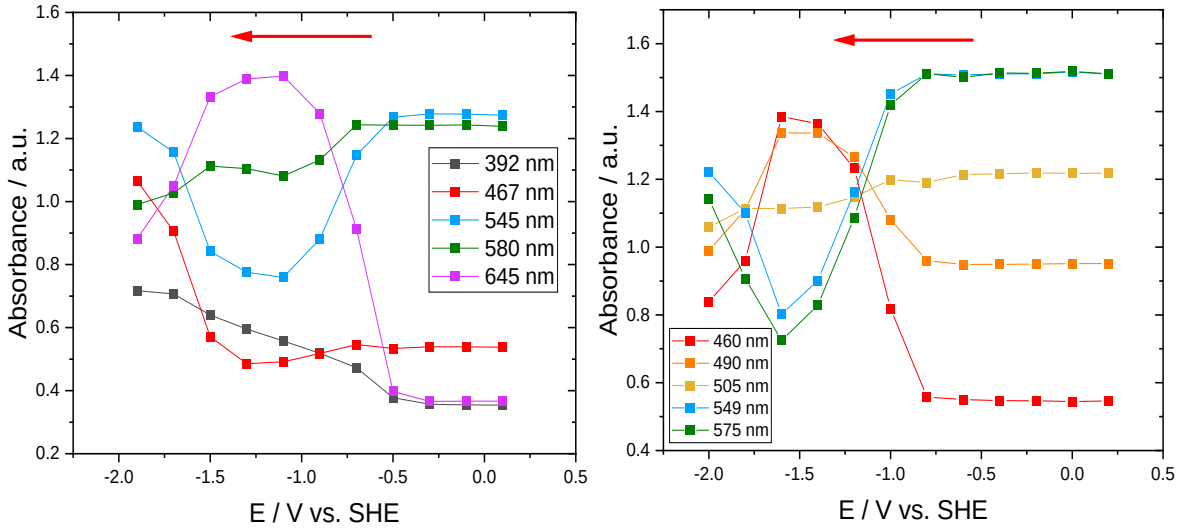

Figure 48: Absorbance vs. Potential plots at corresponding wavelength given of 1,4-Diaminoanthraquinone solution a) under N2 conditions. b) under CO2 conditions.

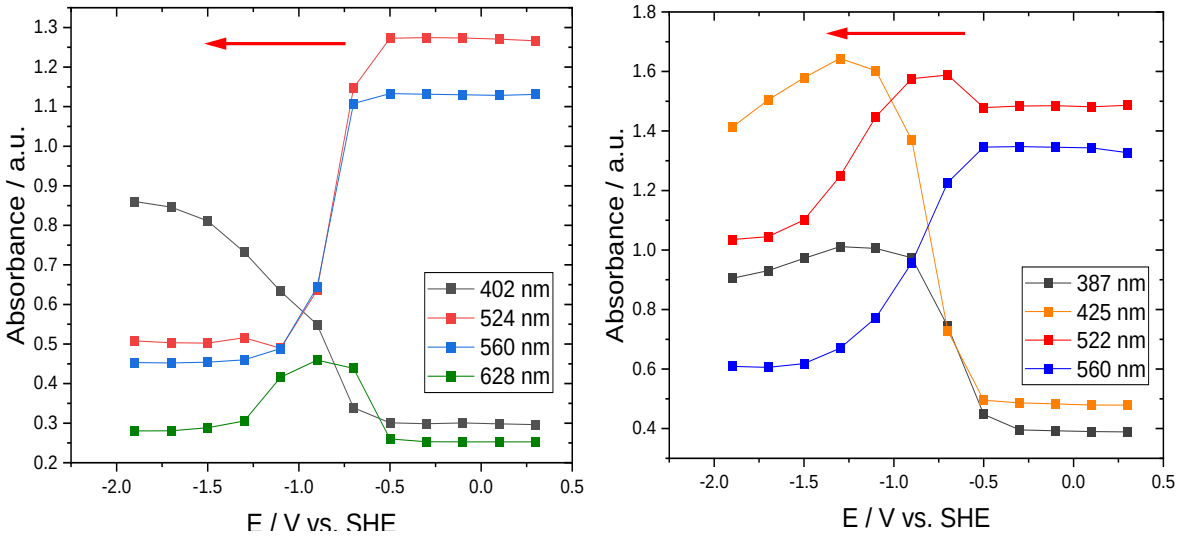

Figure 49: Absorbance vs. Potential plots at corresponding wavelength given of 1-Amino-4-hydroxyanthraquinone solution a) under N2 conditions. b) under CO2 conditions.

Through the Figures above the appearance and disappearance of absorbance bands get better visible. Furthermore, if the graphs under N_2 and CO_2 are compared it is noticeable that certain bands are appearing only under N_2 while others only appear under CO_2.

For the unsubstituted AQ (Figure 43) it is clearly visible that under N_2 as well as under CO_2 the initial band (λ=322 nm) is the only band which is decreasing in the reduction process. Furthermore, the band at 482 nm which is not (clearly) visible in the delta absorbance spectra (Figure 38) shows an earlier increase in absorbance under CO_2 than under N_2. For the AQ all absorbance bands under N_2 and CO_2 remain at the same wavelength and no additional band under CO_2 is appearing. Under CO_2 all bands start increasing at the same potential where the initial band is decreasing. A maximum of the bands at 389, 407, and 482 nm can be found at a potential of approximately -1.4 V. At the end the initial peak is rising again while all the other bands are decreasing.

For the 1-Hydroxyanthraquinone additional bands at 460 and 695 nm appear under CO_2, which were not present under N2. The bands which are also present under N2 were shifted. It is particularly noticeable that all bands under CO2 are increasing. The band above a λ ≥ 600 nm is still present under CO2 which might be an indication for a radical anion but is already too close to the edge of the recorded spectra to provide a detailed answer.

When the plots of the 1-Aminoanthraquinone are compared it is noticeable that under CO_2 bands disappear completely. Under N_2 three initial bands (304, 467, and 495 nm) are present. While the bands at 467 and 495 nm start decreasing at a potential of approximately -1.0 V the band at 304 starts increasing. Under CO_2 the band at 467 nm is decreasing at approximately -0.8 V while the other bands (400, 422, and 557 nm) are increasing to a clear maximum at -1.4 V. A completely new band can be found at 422 nm under CO_2.

Even though the CV of the 1,4-Dihydroxyanthraquinone under CO_2 and N_2 are nearly equal differences in the spectroelectrochemistry can be found. Under CO_2 two completely new bands at 392 and 417 nm are appearing while the bands which are also present under N_2 are shifted. Under N_2 one band at 465 nm is present which is disappeared under CO_2. In both plots a band above 600 nm is visible which indicates the formation of the radical anion as it was also in the case of 1-Hydroxyanthraquinone.

In the case of 1,4-Diaminoanthraquinone two bands are missing under CO_2. One missing band is at 645 nm. When this is compared to the CV this is plausible since there is only one 2 e^- reduction peak. Furthermore, it noticeable that the band at 460 nm under CO_2 appears at a more anodic value (approximately -0.8 V) than under N_2 (approximately -1.5 V).

For the 1-Amino-4-hydroxyanthraquinone under N_2 a band at 628 nm is appearing under N_2 but not under CO_2. This is also the case for the unsubstituted AQ, 1-Aminoanthraquinone, and the 1,4-Diaminoanthraquinone. In addition it is noticed that the band at 522 nm is under N_2 decreasing at a potential of approximately -0.5 V while this band is under CO_2 first increasing and then decreasing. Furthermore, an additional band (λ = 425 nm) is present under CO_2.

To sum it up, three different species regarding the oxidation state are definitely visible for the 1-Hydroxyanthraquinone as well as for the 1,4-Dihydroxyanthraquinone under CO_2. Only for these two molecules a band at a wavelength above 600 nm is visible under CO_2. For the other molecules only one species is present. This is plausible if the plots are compared to the CVs. Furthermore, it is noticeable that in all bands which belong to the second reduction step and therefore indicate the dianion species start increasing at more anodic potential under CO_2 than they appear under N_2. This is also in accordance with the before recorded CVs.

3.6 Electrolysis in aqueous solution

There were only three AQ derivatives which were sufficient soluble in aqueous solution. These AQs have all at least one hydroxy group, which gets deprotonated and the molecule thereby soluble. The anthraquinones with an amino group were not sufficiently soluble in basic or in acidic solution. For electrolysis the highest possible concentration was used. In Table 8 the concentration of the AQ derivative solution were listed.

Table 8: Used AQ derivative concentration for chronoamperometry in NaOH.

Material	**Solubility in NaOH / mmol L^{-1}**
1-Hydroxyaanthraquinone	0.089
1,4-Dihydroxyanthraquinone	0.208
1-Amino-4-hydroxyanthraquinone	0.067

Comparing the colour with the respective anthraquinones dissolved in MeCN a colour change was visible due to deprotonation of the AQ derivatives in alkaline solutions. In Figure 50 the three AQ solution in NaOH were shown.

Figure 50: Colour of 1-Hydroxyanthraquinone (left), 1,4-Dihydroxyanthraquinone (middle), and 1-Amino-4-hydroxyanthraquinone (right).

To see if the colour of the solution will disturb the detection of the H_2O_2 peak at 411 nm UV-vis spectra were recorded before the electrolysis was started. The respective UV-vis spectra are shown in Figure 51-53 .

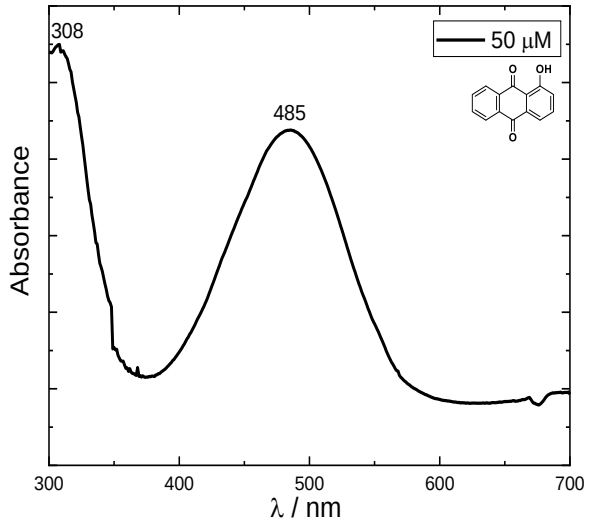

Figure 51: UV-vis spectrum of 1-Hydroxyanthraquinone in NaOH.

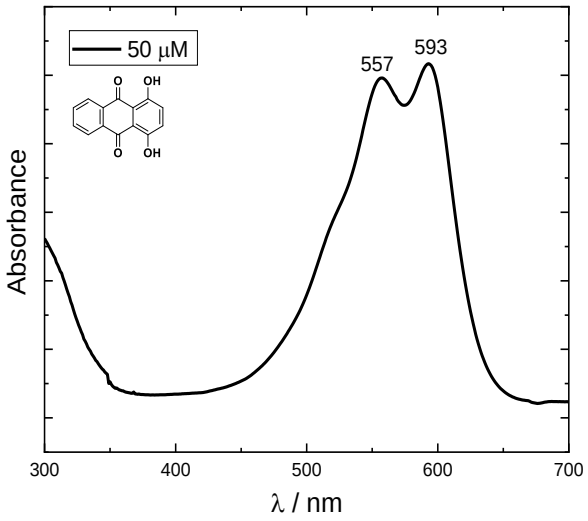

Figure 52: UV-vis spectrum of 1,4-Dihydroxyanthraquinone in NaOH.

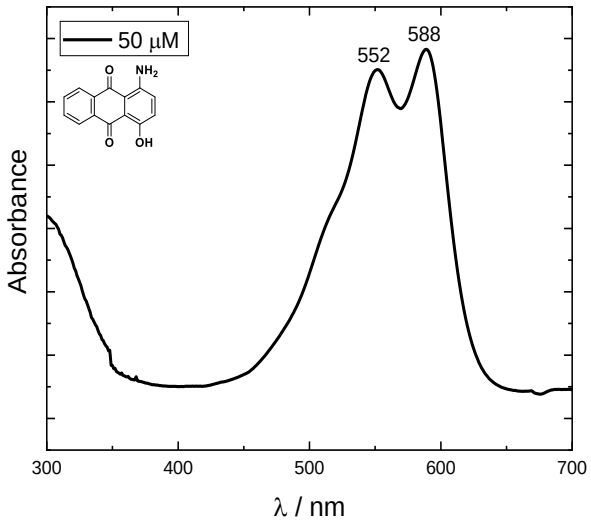

Figure 53: UV-vis spectrum of 1-Amino-4-hydroxyanthraquinone in NaOH.

If these UV-vis spectra in aqueous solution are compared to Figure 18-22 a bathochromic shift can be determined. This shift is related to the solvent where the AQ derivatives were dissolved. In alkaline, aqueous solution the used derivatives are present in their deprotonated form. In Table 9 the absorbance maxima of the molecules which are soluble in MeCN as well as in NaOH are listed.

Table 9: Maximum UV-vis absorbance in MeCN and NaOH.

Molecule	***λ_{max} (in MeCN) / nm***	***λ_{max} (in NaOH) / nm***
1-Hydroxyantraquinone	*400*	*485*
1,4-Dihydroxyanthraquinone	*477*	*593*
1-Amino-4-hydroxyanthraquinone	*567*	*588*

In Figure 54-56 the CVs under N_2 and O_2 of the respective material as well as of the blank GCE can be seen.

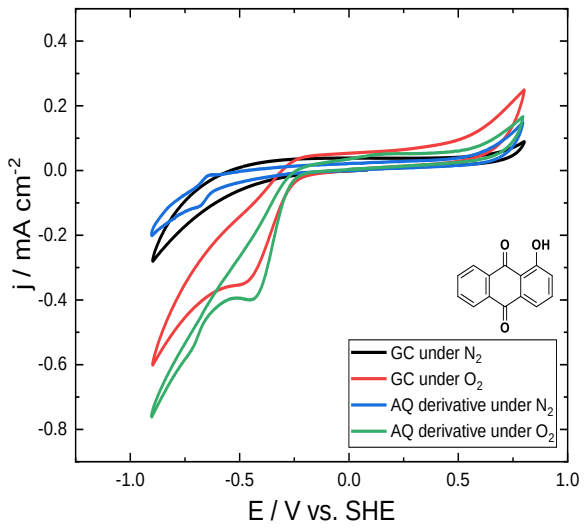

Figure 54: 0.089 M 1-Hydroxyanthraquinone solution vs. blank GCE in NaOH under N_2 and O_2.

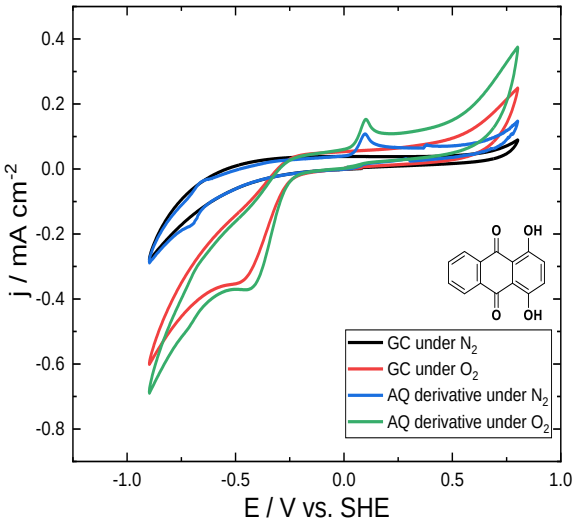

Figure 55: 0.208 M 1,4-Dihydroxyanthraquinone solution vs. blank GCE in NaOH under N_2 and O_2.

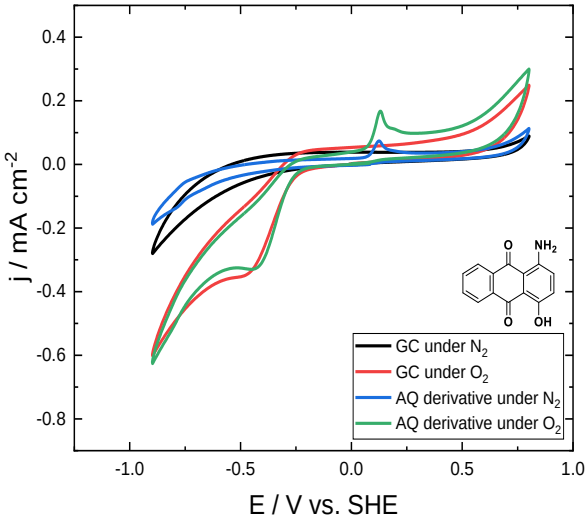

Figure 56: 0.067 M 1-Amino-4-hydroxyanthraquinone solution vs. blank GCE in NaOH under N_2 and O_2.

While the curves under N_2 looks flat, a peak at a potential range of -0.2 to -0.5 V vs. SHE can be observed under O_2. This peak indicates the oxygen reduction of blank GC and that is why at a potential of -400 mV vs. SHE, where a reductive current is present, the chronoamperometry was performed. At the 1-Hydroxyanthraquinone and the 1,4-Dihydroxyanthraquinone the onset of the reduction peak is earlier than at the blank GCE. Furthermore, the peak current is bigger than for the GCE.

Before, the electrolysis with an AQ derivative solution were performed a blank electrolysis with a 0.1 M NaOH was performed. In Figure 57 and 58 the produced amount of peroxide and the Faraday efficiency compared to the blank GCE are shown.

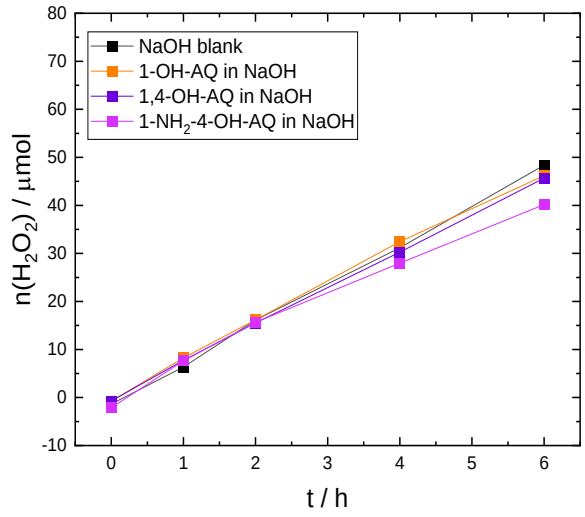

Figure 57: Produced hydrogen peroxide over a time of 6 h in NaOH.

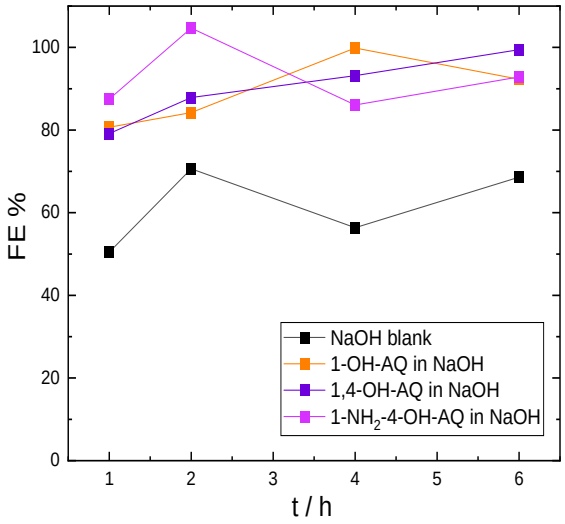

Figure 58: Faraday efficiency of each material in NaOH.

In Table 10 the produced amount of H_2O_2 after 6 h electrolysis and the average faraday efficiency are listed for each material as well as for the blank GCE.

Table 10: Produced amount of hydrogen peroxide and Faraday efficiency of the used materials in NaOH.

Material	**Produced amount of H_2O_2 / µmol**	**Average faraday efficiency / %**
Blank GCE	48.4	62.5
1-Hydroxyanthraquinone	46.2	89.3
1,4-Dihydroxyanthraquinone	45.7	89.9
1-Amino-4-hydroxyanthraquinone	40.2	92.8

The blank GCE produced nearly 50 µmol H_2O_2 with an average faraday efficiency of 63 %. In the Figures above it can be observed that all anthraquinones produce slightly less amount of peroxide than the blank GCE but with a higher faraday efficiency. It is surprising that the solutions containing an AQ derivative produce less amount peroxide as the blank GCE. It was

suspected that the AQs catalyse the reaction. Even though the 1-Hydroxyanthraquinone and the 1,4-Dihydroxyanthraquinone produce approximately as much peroxide as the blank GCE the mixed anthraquinone produces noticeable less. Generally, it was suspected that the AQ derivative solution will produce a higher amount of peroxide than the GCE.

During the chronoamperometry of the AQ derivative solutions in NaOH as well as of the blank NaOH solution samples were taken after 0, 1, 2, 4, and 6 h to record the production hydrogen peroxide over this time period. In Figure 59 the delta absorbance spectra of the H_2O_2 detection in a 0.089 mM 1-Hydroxyanthraquinone solution is shown. In the spectra only one peak with a maximum at a wavelength of 413 nm is visible. This peak belongs to the absorbance of H_2O_2 and is increasing over the time of electrolysis. All used AQ derivatives are not visible in the respective delta absorbance spectra.

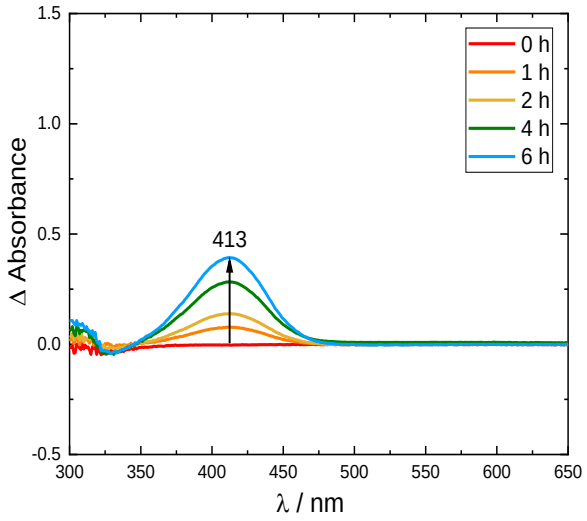

Figure 59: Delta absorbance spectrum of H2O2 detection in a 1-Hydroxyanthraquinone solution.

3.7 Electrolysis in non-aqueous solution

In Figure 60 to 65 the CVs of a 2 mM AQ derivative solution in MeCN under N_2 and O_2 are shown in comparison to the blank GCE.

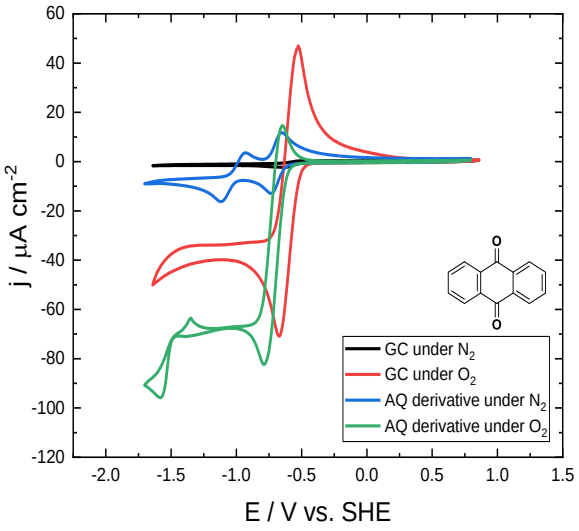

Figure 60: Anthraquinone vs. blank GCE in MeCN solution under N_2 and O_2.

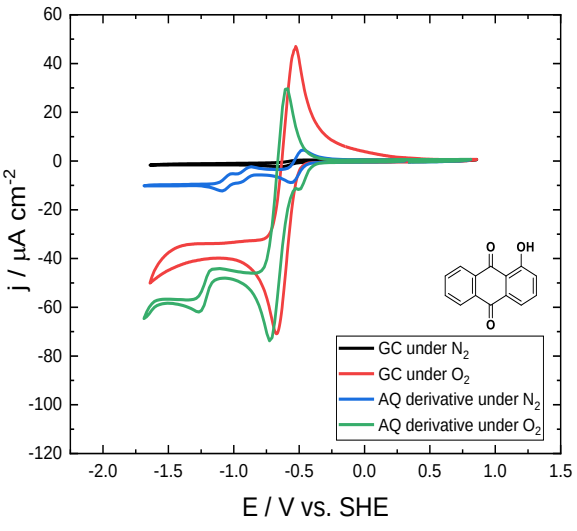

Figure 61: 1-Hydroxyanthraquinone vs. blank GCE in MeCN solution under N_2 and O_2.

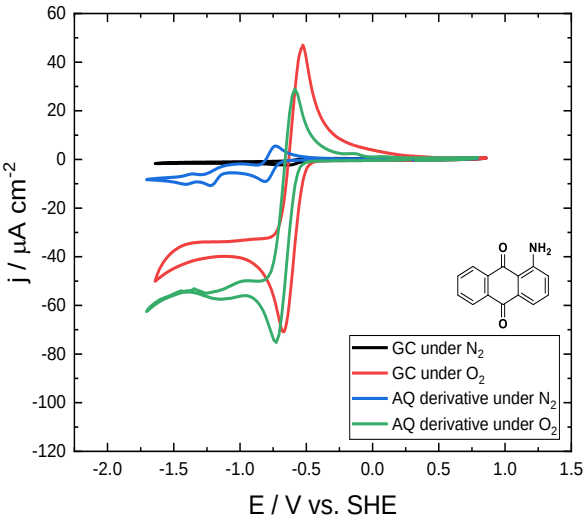

Figure 62: 1-Aminoanthraquinone vs. blank GCE in MeCN solution under N_2 and O_2.

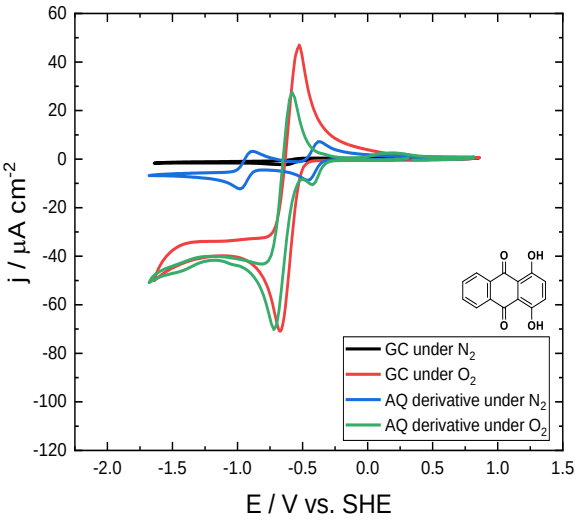

Figure 63: 1,4-Dihydroxyanthraquinone vs. blank GCE in MeCN solution under N_2 and O2.

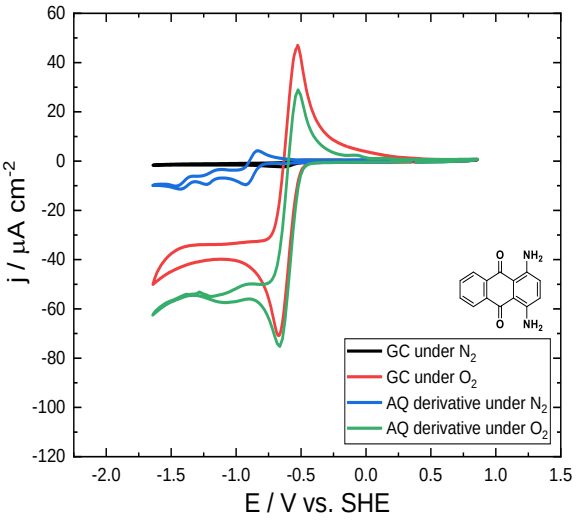

Figure 64: 1,4-Diaminoanthraquinone vs. blank GCE in MeCN solution under N_2 and O_2.

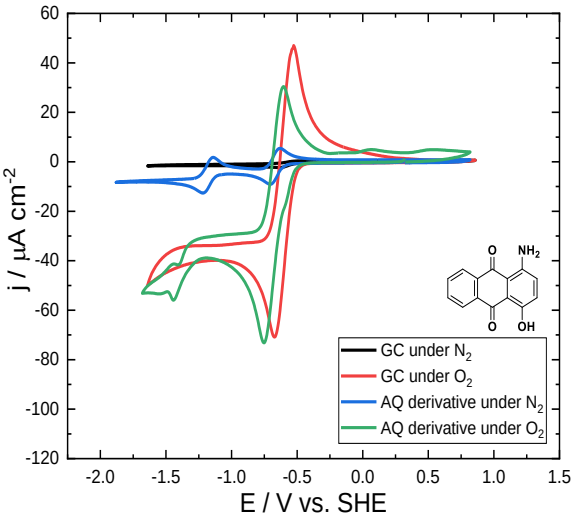

Figure 65: 1-Amino-4-hydroxyanthraquinone vs. blank GCE in MeCN solution under N_2 and O_2.

The CVs of the AQ derivatives under N_2 show as mentioned in chapter 1.4 the two one electron reduction steps. While the CVs under O_2 show only one big peak for the oxygen reduction. In the case of the 1-Hydroxanthraquinone and the 1,4-Dihydroxyanthraquinone a small peak is visible before the oxygen reduction peak. This peak is from the first reduction of the AQ derivative. Additionally, this peak show under O_2 a higher current as under N_2. Compared to the peak of the blank GCE (-0.65 V) it is visible that the reduction peak is shifted cathodically (-0.72 V). If then the recorded CVs in MeCN are compared to the ones in NaOH (chapter 3.4) it is visible that the peak which indicated the oxygen reduction is shifted to more cathodic values. As the O_2 reduction was in NaOH at a potential of -0.4 V vs. SHE the reduction peak is at a potential of approximately -0.65 V vs. SHE for the blank GCE and at a potential of approximately -0.72 V for the AQ derivatives.

In Figure 66 and 67 again the production and faraday efficiency vs. time are shown.

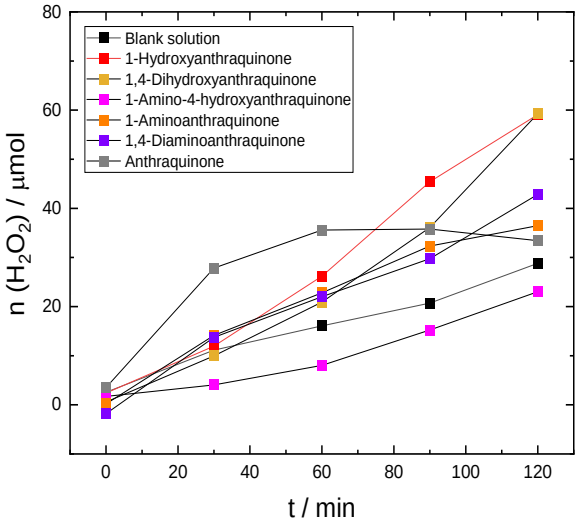

Figure 66: Produced amount of hydrogen peroxide over a time of 120 min in MeCN.

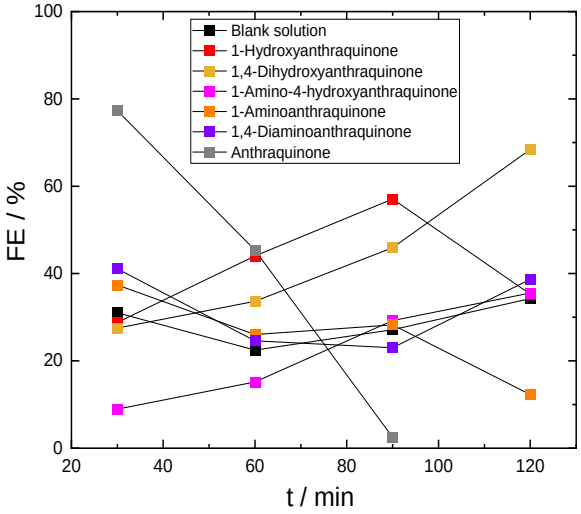

Figure 67: Faraday efficiency of all materials in MeCN.

In Table 11 the produced amount of H_2O_2 (after 120 min electrolysis) as well as the average faraday efficiency of the materials are listed.

Table 11: Produced amount of hydrogen peroxide and Faraday efficiency of the used materials in MeCN.

Material	Produced amount of H_2O_2 / µmol	Average faraday efficiency / %
Blank GCE	28.8	28.7
Anthraquinone	33.4	-
1-Hydroxyanthraquinone	59.1	41.3
1-Aminoanthraquinone	36.5	26.0
1,4-Dihydroxyanthraquinone	59.3	43.9
1,4-Diaminoanthraquinone	42.8	25.2
1-Amino-4-hydroxyanthraquinone	23.0	19.7

The blank GCE values are used as reference value. Compared to this it is noticeable that all AQ derivatives except the 1-Amino-4-hydroxyanthraquinone produces more µmol H_2O_2. The 1-Hydroxyanthraquinone and the 1,4-Dihydroxyanthraquinone produce the most, with an amount of approximately 59 µmol. The 1-Amino-4-hydroxyanthraquinone is the one with the lowest H_2O_2 production.

When comparing the faraday efficiency of the single materials and the blank GCE it is noticeable that only the 1-Hydroxyanthraquinone and the 1,4-Dihydroxyanthraquinone have a higher faraday efficiency. If the 1,4-Dihydroxyanthraquinone faraday efficiency is viewed in Figure 64, an activation period is recognizable. With the 1-Hydroxyanthraquinone in contrast it is remarkable that the faraday efficiency is steady increasing in the first 90 min and in the last 30 min it is rapidly decreasing which, however, does not affect the produced amount of H_2O_2.

Especially, in Figure 65 the unsubstituted AQ stand out. The faraday efficiency of the AQ starts at 80 % and then drastically decreasing towards 0. If the production is considered it is visible that the amount of H_2O_2 is steady increasing in the first half of the chronoamperometry. In the second half the amount of H_2O_2 is decreasing. This means that the produced peroxide is decomposed in the last hour.

During the chronoamperometry of the AQ derivative solutions in MeCN as well as of the blank MeCN solution samples were taken after 0, 30, 60, 90, and 120 min to record the production hydrogen peroxide over this time period. In Figure 68-73 the delta absorbance spectra of the H_2O_2 detection in a 2 mM AQ derivative solution are shown. In the spectra the H_2O_2 peak at 413 nm is visible. This peak increases over time which indicates a successful production of hydrogen peroxide. Furthermore, the decreasing of the AQ derivative is also visible in Figure 70-73.

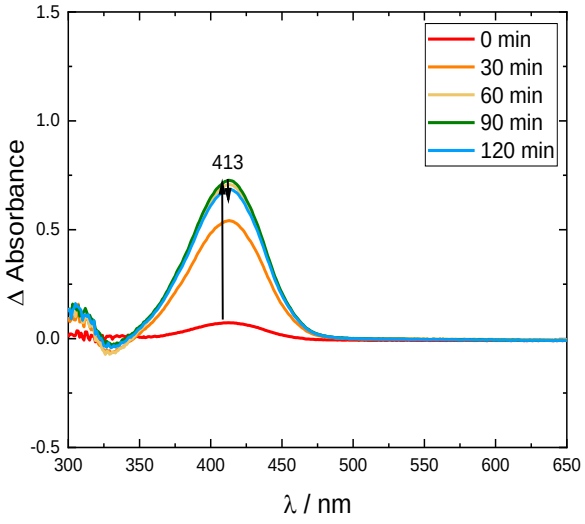

Figure 68: Delta absorbance spectra of the H_2O_2 production in a AQ solution.

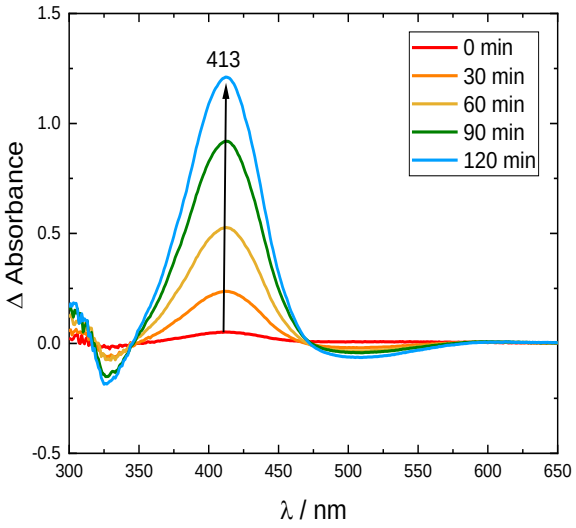

Figure 69: Delta absorbance spectra of the H_2O_2 production in a 1-Hydroxyanthraquinone solution.

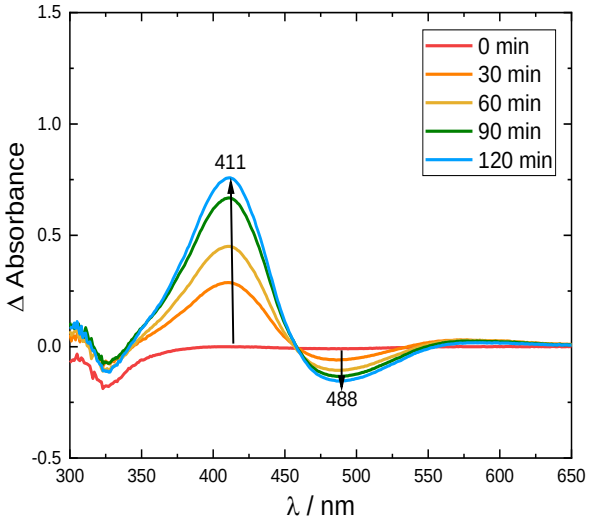

Figure 70: Delta absorbance spectra of the H_2O_2 production in a 1-Aminoanthraquinone solution.

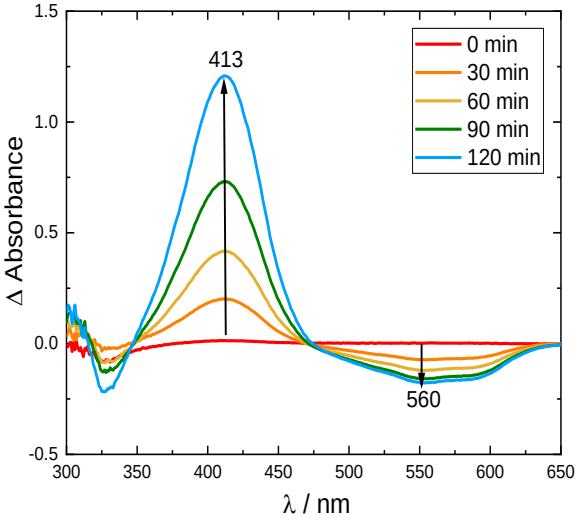

Figure 71: Delta absorbance spectra of the H_2O_2 production in a 1,4-Dihydroxyanthraquinone solution.

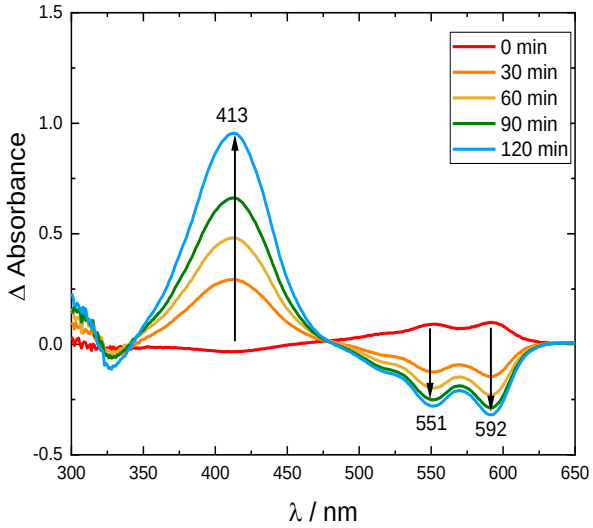

Figure 72: Delta absorbance spectra of the H_2O_2 production in a 1,4-Diaminoanthraquinone solution.

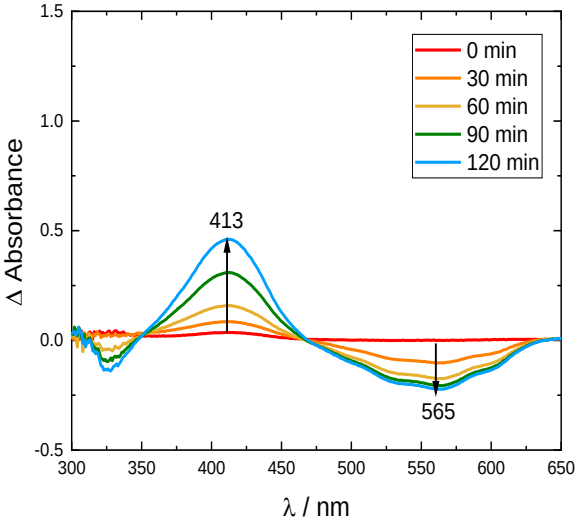

Figure 73: Delta absorbance spectra of the H_2O_2 production in a 1-Amino-4-hydroxyanthraquinone solution.

4. Conclusion

On the one hand this thesis aimed for a better understanding of the anthraquinone CO_2 interaction and the underlaying mechanism. Through the high cathodic current which was observed in the CV under CO_2 the question if AQ derivatives reduce or capture CO_2 occurred. Since this current decreased in in each additional cycle and is also appearing in a blank MeCN solution it was suggested that the potential window was exceed and this current was caused by the WE. The chronoamperometry with subsequent GC analysis proved this suggestion since there was no CO detected.

Through the comparison of the CVs under N_2 and CO_2 it was noticeable that the second reduction peak is shifted towards more anodic potentials and merged with the first. For better understanding of this mechanism the spectroelectrochemistry was performed under N_2 and CO_2. Here, it was particularly noticeable that some absorbance bands only appear under N_2 and some only under CO_2 while certain bands appear in both measurements. Especially, the band above 600 nm which is considered as the radical anion is missing in all spectra under CO_2 except the spectrum of the 1-Hydroxyanthraquinone and the 1,4-Diaminoanthraquinone. This conforms the assumption that amino substituted AQs are more reactive under CO_2 than the hydroxy substituted ones. Furthermore, it is noticed that the absorbance bands which are indicated as the ones for the dianion appear under CO2 at more anodic potentials as under N_2. To prove this definitively, further work with spectroscopy or quantum mechanical calculations are needed.

On the other hand of this thesis the electrochemical production of H_2O_2 was investigated. At the beginning of this experiment it was suspected that the AQ derivative should catalyse the H_2O_2 production. Nevertheless, the chronoamperometry in aqueous AQ derivative solution did not verify this assumption. Since all derivatives produce less amount H_2O_2 than the blank GCE (48 µmol). However, the pure hydroxy substituted derivatives produced nearly the same amount of H_2O_2 (46 µmol) while the 1-Amino-4-hydroxyanthraquinone produced significantly less (40 µmol). If the Faraday efficiency is considered all AQ derivatives show a higher averaged FE than the blank GCE. Although less amount of H_2O_2 was produced, the FE is significantly higher, which can also be considered as electrocatalytic.

In non-aqueous solution all AQ derivatives except the 1-Amino-4-hydroxy produce a higher amount of H_2O_2. If the Faraday efficiencies are compared it is noticed that only the pure hydroxy substituted AQs have a higher FE in average than the GCE. Remarkable is that the 1-Hydroxyanthraquinone and the 1,4-Dihydroxyanthraquione in non-aqueous solution produce a higher amount of hydrogen peroxide (59 µmol) in 2 h than in 6 h in aqueous solution (46 µmol).

To sum it up, the amino substituted AQs are better suitable for the CO_2 capturing. Since they are more reactive under CO_2 which is proven through the absence of the radical anion band in the UV-vis absorbance spectrum under CO_2. Furthermore, this groups and the unsubstituted AQ show an additional peak in a potential range of -1.45 and -1.7 V which indicates an interaction between the AQ derivative and CO_2. In contrast to the CO_2 capturing the hydroxy

substituted AQ derivatives are more suitable for production of H_2O_2 due to the higher amount of produced H_2O_2 as well as the higher Faraday efficiency, which is in accordance to literature reports.

5. Appendix

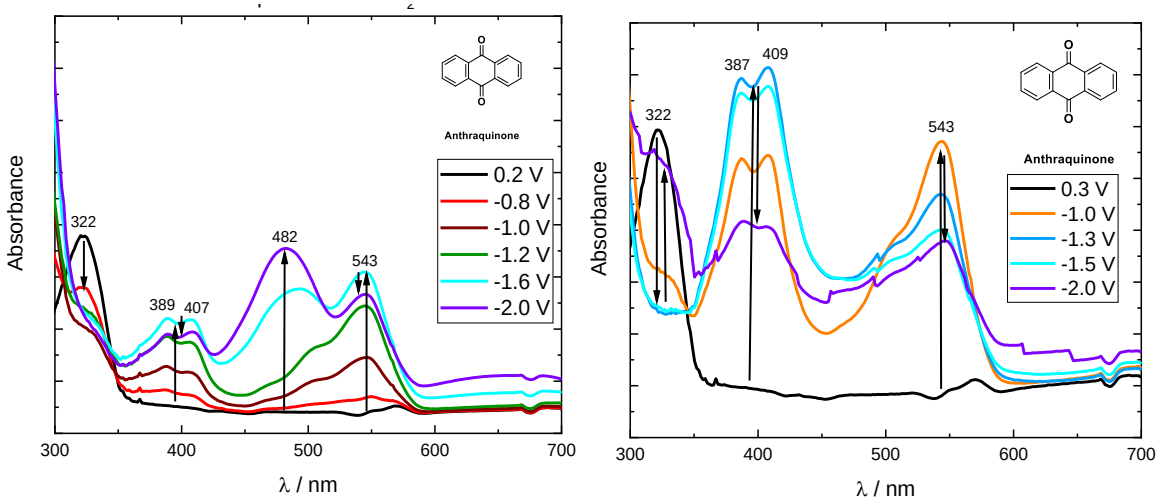

Figure 74:UV-vis absorbance spectra of AQ a) under N_2 conditions. b) under CO_2 conditions.

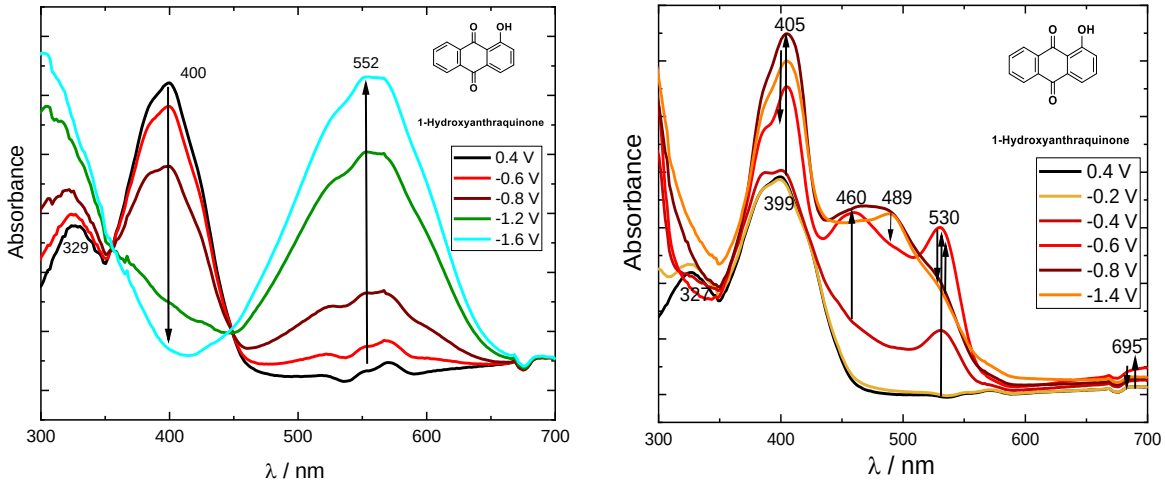

Figure 75Figure 74: UV-vis absorbance spectra of 1-Hydroxyanthraquinone a) under N_2 conditions. b) under CO_2 conditions.

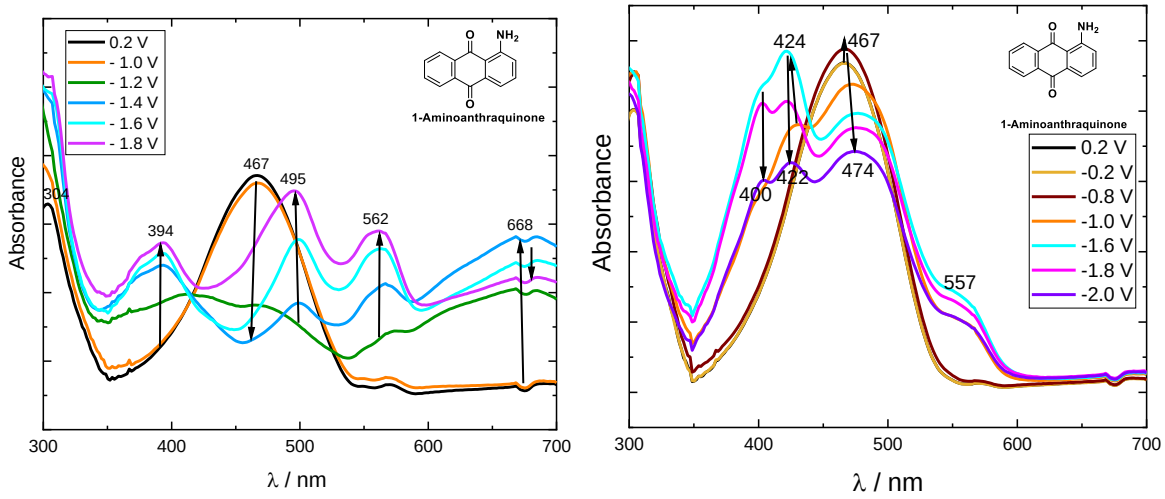

Figure 76: Figure 74: UV-vis absorbance spectra of 1-Aminoanthraquinone a) under N_2 conditions. b) under CO_2 conditions.

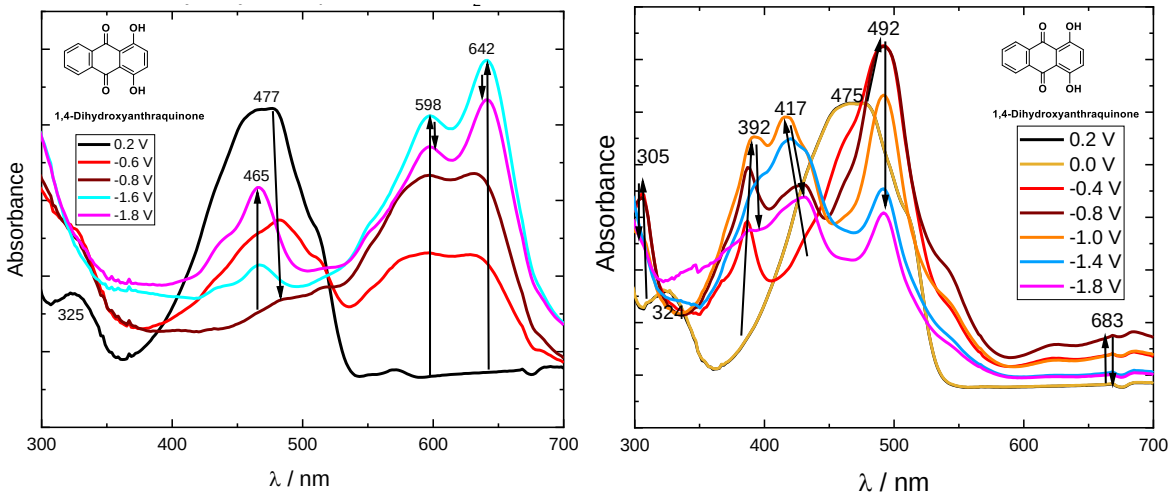

Figure 77: Figure 74: UV-vis absorbance spectra of 1,4-Dihydroxyanthraquinone a) under N_2 conditions. b) under CO_2 conditions.

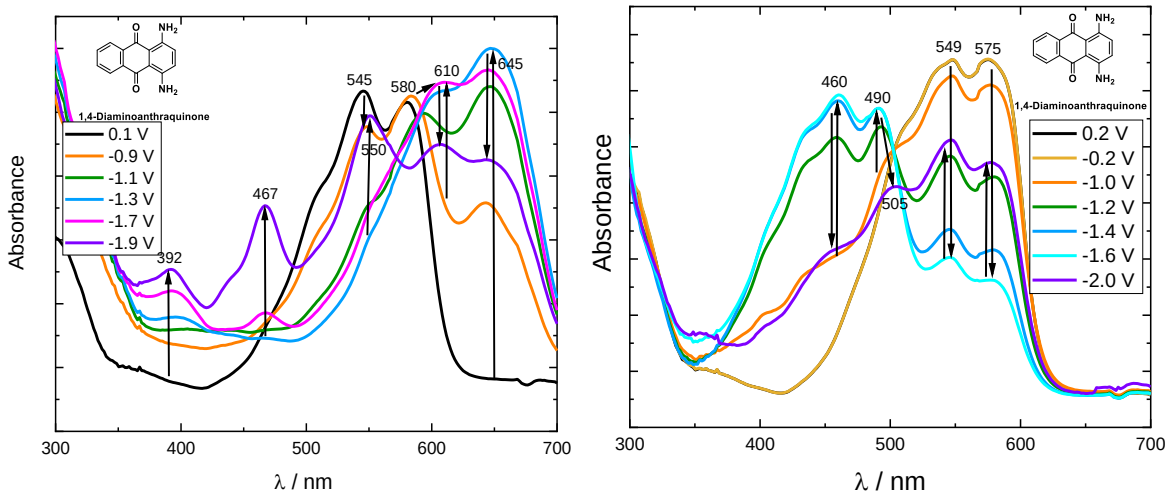

Figure 78: Figure 74: UV-vis absorbance spectra of 1,4-Diaminoanthraquinone a) under N_2 conditions. b) under CO_2 conditions.

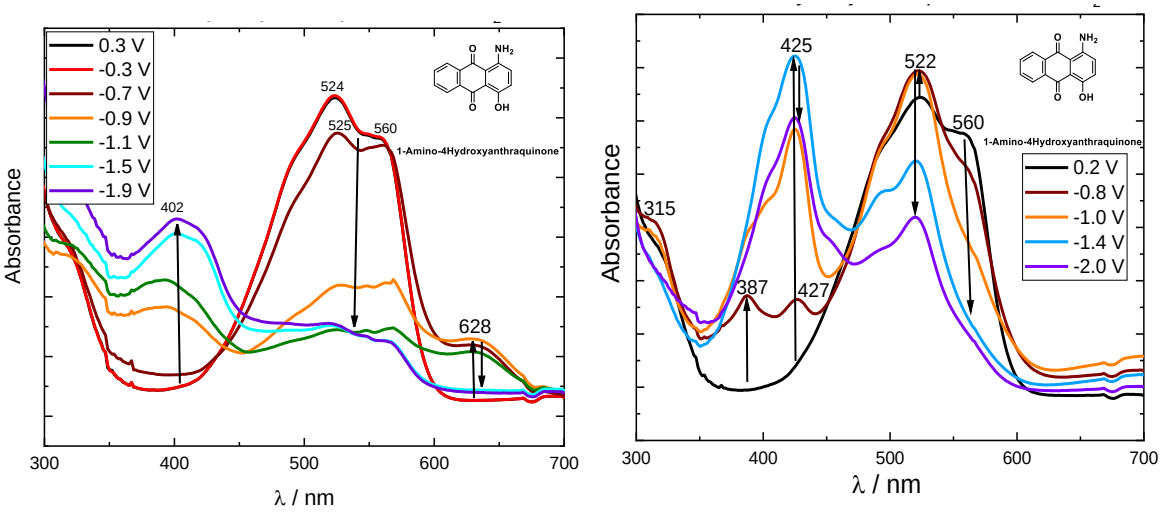

Figure 79: Figure 74: UV-vis absorbance spectra of 1-Amino-4-hydroxyanthraquinone a) under N_2 conditions. b) under CO_2 conditions.

6. Literature

(1) Mathews, A. P. Renewable Energy Technologies: Panacea for World Energy Security and Climate Change? *Procedia Comput. Sci.* **2014**, *32*, 731–737. https://doi.org/10.1016/j.procs.2014.05.483.

(2) Adedoyin, F.; Ozturk, I.; Abubakar, I.; Kumeka, T.; Folarin, O.; Bekun, F. V. Structural Breaks in CO2 Emissions: Are They Caused by Climate Change Protests or Other Factors? *J. Environ. Manage.* **2020**, *266* (December 2019), 110628. https://doi.org/10.1016/j.jenvman.2020.110628.

(3) Dincer, I. Renewable Energy and Sustainable Development: A Crucial Review. *Renew. Sustain. energy Rev.* **2000**, *4* (2), 157–175. https://doi.org/10.1016/S1364-0321(99)00011-8.

(4) Olesen; Bindi. Consequences of Climate Change for European Agricultural Productivity, land use and policy. *European Journal of Agronomy.* **2002**, *16*, 239–262. https://doi.org/10.1016/S1161-0301(02)00004-7.

(5) Rizakulyevna, C. M. Alternative Energy Sources. *The American Journal of Applied Science.* **2021**, *03* (01), 58–68. https://doi.org/10.37547/tajas/Volume03Issue01-11.

(6) Panwar, N. L.; Kaushik, S. C.; Kothari, S. Role of Renewable Energy Sources in Environmental Protection : A Review. *Renew. Sustain. Energy Rev.* **2011**, *15* (3), 1513–1524. https://doi.org/10.1016/j.rser.2010.11.037.

(7) Rosen, M. A. A Review of Energy Storage Types , Applications and Recent Developments. *J. Energy Storage* **2020**, *27* (July 2019), 101047. https://doi.org/10.1016/j.est.2019.101047.

(8) Yoro, K. O.; Daramola, M. O. 1. *CO2 Emission Sources, Greenhouse Gases, and the Global Warming Effect*. *Advances in Carbon Capture Methods, Technologies and Applications.* **2020**, 3-28. https://doi.org/10.1016/b978-0-12-819657-1.00001-3.

(9) Waheed, R.; Chang, D.; Sarwar, S.; Chen, W. Forest , Agriculture , Renewable Energy , and CO2 Emission. *J. Clean. Prod.* **2018**, *172*, 4231–4238. https://doi.org/10.1016/j.jclepro.2017.10.287.

(10) Machado, K. S.; Seleme, R.; Maceno, M. M. C.; Zattar, I. C. Carbon Footprint in the Ethanol Feedstocks Cultivation – Agricultural CO 2 Emission Assessment. *Agric. Syst.* **2017**, *157* (December 2016), 140–145. https://doi.org/10.1016/j.agsy.2017.07.015.

(11) Samipour, S.; Ahmadi, A.; Manshadi, M. D. 19. *Challenges in Industrialization of Biological CO2 Capture*. *Advances in Carbon Capture Methods, Technologies and Applications.* **2020**, 431-451. https://doi.org/10.1016/B978-0-12-819657-1.00019-0.

(12) Bhattacharya, M.; Awaworyi, S.; Reddy, S. The Dynamic Impact of Renewable Energy and Institutions on Economic Output and CO2 Emissions across Regions. *Renew. Energy* **2017**, *111*, 157–167. https://doi.org/10.1016/j.renene.2017.03.102.

(13) Patricio, J.; Angelis-Dimakis, A.; Castillo-Castillo, A.; Kalmykova, Y.; Rosado, L. Method to Identify Opportunities for CCU at Regional Level - Matching Sources and Receivers. *J. CO2 Util.* **2017**, *22* (September), 330–345. https://doi.org/10.1016/j.jcou.2017.10.009.

(14) Environ, E.; Ferrari, M.; Gross, R.; Hallett, J. P. Carbon Capture and Storage Update. *Energy Environ. Sci.* **2014**, 7, 130-189. https://doi.org/10.1039/c3ee42350f.

(15) Panwar, N. L.; Kaushik, S. C.; Kothari, S. Role of Renewable Energy Sources in Environmental Protection: A Review. *Renew. Sustain. Energy Rev.* **2011**, *15* (3), 1513–1524. https://doi.org/10.1016/j.rser.2010.11.037.

(16) Apaydin, D. H.; Gora, M.; Portenkirchner, E.; Oppelt, K. T.; Neugebauer, H.; Jakesova, M.; Glowacki, E. D.; Kunze-Liebhäuser, J. Electrochemical Capture and Release of CO2 in Aqueous Electrolytes Using an Organic Semiconductor Electrode. *ACS Appl. Mater. Interfaces.* **2017**, 9, 15, 12919–12923. https://doi.org/10.1021/acsami.7b01875.

(17) Schlager, S.; Dibenedetto, A.; Aresta, M.; Apaydin, D. H.; Neugebauer, H.; Sariciftci, N. S. Biocatalytic and Bioelectrocatalytic Approaches for the Reduction of Carbon Dioxide Using Enzymes. *Energy Technology Generation, Conversion, Storage, Distribution.* **2017**, 5 (6). https://doi.org/10.1002/ente.201600610.

(18) Apaydin, D. H.; Schlager, S.; Portenkirchner, E. Organic , Organometallic and Bioorganic Catalysts for Electrochemical Reduction of CO2. **2017**, 3094–3116. https://doi.org/10.1002/cphc.201700148.

(19) Apaydin, D. H.; Głowacki, E. D.; Portenkirchner, E.; Sariciftci, N. S. Direct Electrochemical Capture and Release of Carbon Dioxide Using an Industrial Organic Pigment: Quinacridone. *Angew. Chemie - Int. Ed.* **2014**, *53* (26), 6819–6822. https://doi.org/10.1002/anie.201403618.

(20) Wielend, D.; Apaydin, D. H.; Sariciftci, N. S. Anthraquinone Thin-Film Electrodes for Reversible CO2 Capture and Release. *J. Mater. Chem. A* **2018**, *6* (31), 15095–15101. https://doi.org/10.1039/c8ta04817g.

(21) Yin, W.; Grimaud, A.; Azcarate, I.; Yang, C.; Tarascon, J. M. Electrochemical Reduction of CO2 Mediated by Quinone Derivatives: Implication for Li-CO2 Battery. *J. Phys. Chem. C* **2018**, *122* (12), 6546–6554. https://doi.org/10.1021/acs.jpcc.8b00109.

(22) Gurkan, B.; Simeon, F.; Hatton, T. A. Quinone Reduction in Ionic Liquids for Electrochemical CO2 Separation. *ACS Sustain. Chem. Eng.* **2015**, *3* (7), 1394–1405. https://doi.org/10.1021/acssuschemeng.5b00116.

(23) Tam, S. M.; Tessensohn, M. E.; Tan, J. Y.; Subrata, A.; Webster, R. D. Competition between Reversible Capture of CO2and Release of CO2•-Using Electrochemically Reduced Quinones in Acetonitrile Solutions. *J. Phys. Chem. C* **2021**, *125* (22), 11916–11927. https://doi.org/10.1021/acs.jpcc.1c00997.

(24) Lee, J.; Jeong, B.; Ocon, J. D. Oxygen Electrocatalysis in Chemical Energy Conversion and Storage Technologies. *Curr. Appl. Phys.* **2013**, *13* (2), 309–321. https://doi.org/10.1016/j.cap.2012.08.008.

(25) Ge, X.; Sumboja, A.; Wuu, D.; An, T.; Li, B.; Goh, F. W. T.; Hor, T. S. A.; Zong, Y.; Liu, Z. Oxygen Reduction in Alkaline Media : From Mechanisms to Recent Advances of Catalysts. *ACS Catal.* **2015**, 5, 8, 4643–4667. ttps://doi.org/10.1021/acscatal.5b00524.

(26) Sa, C. M.; Bard, A. J. Hydrogen Peroxide Production in the Oxygen Reduction Reaction at Different Electrocatalysts as Quantified by Scanning Electrochemical Microscopy. **2009**, *81* (19), 8094–8100.

(27) Wielend, D.; Neugebauer, H.; Sariciftci, N. S. Revealing the Electrocatalytic Behaviour by a Novel Rotating Ring-Disc Electrode (RRDE) Subtraction Method: A Case-Study on Oxygen Reduction Using Anthraquinone Sulfonate. *Electrochem. commun.* **2021**, *125* (February), 106988. https://doi.org/10.1016/j.elecom.2021.106988.

(28) Jung, E.; Shin, H.; Antink, W. H.; Sung, Y.; Hyeon, T. Recent Advances in Electrochemical Oxygen. *Energy Lett.* **2020**, 5, 6, 1881–1892 https://doi.org/10.1021/acsenergylett.0c00812.

(29) Jorge, P.; Cordeiro-junior, M.; Schiavon, M.; Athie, L.; Carolina, N.; Helena, L.; Coelho, M.; Bertazzoli, R.; Roberto, M.; Lanza, D. V. Catalysis of Oxygen Reduction Reaction for H2O2 Electrogeneration : The Impact of Different Conductive Carbon Matrices and Their Physicochemical Properties. *J. Catal.* **2020**, *392*, 56–68. https://doi.org/10.1016/j.jcat.2020.09.020.

(30) An, L.; Zhao, T.; Yan, X. The Dual Role of Hydrogen Peroxide in Fuel Cells. Sci. Bull, **2015**, *60*, 55–64. https://doi.org/10.1007/s11434-014-0694-7.

(31) Fukuzumi, S. Artificial Photosynthesis for Production of Hydrogen Peroxide and Its Fuel Cells. *Biochimica et Biophysica Acta (BBA) Bioenergetics.* **2016**, *1857* (5), 604–611. https://doi.org/10.1016/j.bbabio.2015.08.012.

(32) Campos-Martin, J. M.; Blanco-Brieva, G.; Fierro, J. L. G. Hydrogen Peroxide Synthesis : An Outlook beyond the Anthraquinone Process. *Angewandte Chemie*. **2006**, 6962–6984. https://doi.org/10.1002/anie.200503779.

(33) Samanta, C.; Choudhary, V. R. Direct Formation of H2O2 from H2 and O2 and Decomposition / Hydrogenation of H2O2 in Aqueous Acidic Reaction Medium over Halide-Containing Pd / SiO2 Catalytic System. *Catalytic Communications.* **2007**, *8 (12)*, 2222–2228. https://doi.org/10.1016/j.catcom.2007.05.007.

(34) Jiang, Y.; Ni, P.; Chen, C.; Lu, Y.; Yang, P.; Kong, B.; Fisher, A.; Wang, X. Selective Electrochemical H2O2 Production through Two-Electron Oxygen Electrochemistry. *Advanced Energy Materials.* **2018**, 8 (31), 17–19. https://doi.org/10.1002/aenm.201801909.

(35) Lim, J.; Hoffmann, M. R. Substrate Oxidation Enhances the Electrochemical Production of Hydrogen Peroxide. *Chem. Eng. J.* **2019**, *374* (February), 958–964. https://doi.org/10.1016/j.cej.2019.05.165.

(36) Kung, M. C.; Kung, H. H. Prospect of Vapor Phase Catalytic H2O2 Production by Oxidation of Water. *Chinese J. Catal.* **2019**, *40* (11), 1673–1678. https://doi.org/10.1016/S1872-2067(19)63327-9.

(37) Goor, G.; Glenneberg, J.; Jacobi, S. Hydrogen, 1.Properties and Occurence. Ullmann's Encycl. Ind. Chem. **2000**, 394–427. https://doi.org/10.1002/14356007.a13.

(38) Shi, X.; Back, S.; Gill, T. M.; Siahrostami, S.; Zheng, X. Review Electrochemical Synthesis of H2O2 by Two-Electron Water Oxidation Reaction. *CHEMPR* **2021**, *7* (1), 38–63. https://doi.org/10.1016/j.chempr.2020.09.013.

(39) Wernimont, E.; Ventura, M.; Garboden, G.; Mullens, P. Past and Present Uses of Rocket Grade Hydrogen Peroxide. *Kinetics*, **1999**, 1–15.

(40) Diaz-Munoz, G.; Miranda, I. L. 11. Anthraquinones : An Overview. *Studies in Natural Products Chemistry.* **2018**, *58*, 313-338. https://doi.org/10.1016/B978-0-444-64056-7.00011-8.

(41) Phillips, M.; The Chemistry of Anthraquinone. *Chem. Rev.* **1929**, 6 (1), 157–174. https://doi.org/10.1021/cr60021a007.

(42) Morin, J. Recent Advances in the Chemistry of Vat Dyes. *J. Mater. Chem. C.* **2017**, 12298–12307. https://doi.org/10.1039/c7tc03926c.

(43) Roessler, A.; Dossenbach, O.; Marte, W.; Rys, P. Electrocatalytic Hydrogenation of Vat Dyes. *Dyes und Pigments.* **2002**, *54*, 141–146. https://doi.org/10.1016/S0143-7208(02)00035-9.

(44) Osugi, M. E.; Rajeshwar, K.; Ferraz, E. R. A.; Oliveira, D. P. De; Araújo, Â. R.; Valnice, M.; Zanoni, B. Comparison of Oxidation Efficiency of Disperse Dyes by Chemical and Photoelectrocatalytic Chlorination and Removal of Mutagenic Activity. *Electrochemica Acta*. **2009**, *54*, 2086–2093. https://doi.org/10.1016/j.electacta.2008.07.015.

(45) Szpyrkowicz, L.; Juzzolino, C.; Kaul, S. N.; Daniele, S.; Faveri, M. D. De. Electrochemical Oxidation of Dyeing Baths Bearing Disperse Dyes. *Ind. Eng. Chem. Res*. **2000**, 3241–3248. https://doi.org/10.1021/ie9908480

(46) Zarren, G.; Nisar, B.; Sher, F. Materials Today Sustainability Synthesis of Anthraquinone-Based Electroactive Polymers : A Critical Review. *Mater. Today Sustain.* **2019**, *5*, 100019. https://doi.org/10.1016/j.mtsust.2019.100019.

(47) He, D.; Chen, B.; Tian, Q.; Yao, S. Journal of Pharmaceutical and Biomedical Analysis Simultaneous Determination of Five Anthraquinones in Medicinal Plants and Pharmaceutical Preparations by HPLC with Fluorescence Detection. *Journal of Pharmaceutical and Biomedical Analysis.* **2009**, *49*, 1123–1127. https://doi.org/10.1016/j.jpba.2009.02.014.

(48) Malik, E. M.; Christa, E. M. Tools and Drugs. *Medical research reviews*. **2016**, No. 4, 705–748. https://doi.org/10.1002/med.

(49) Shamsipur, M.; Siroueinejad, A.; Hemmateenejad, B.; Abbaspour, A.; Sharghi, H.; Alizadeh, K.; Arshadi, S. Cyclic Voltammetric, Computational, and Quantitative Structure-Electrochemistry Relationship Studies of the Reduction of Several 9,10-Anthraquinone Derivatives. *J. Electroanal. Chem.* **2007**, *600* (2), 345–358. https://doi.org/10.1016/j.jelechem.2006.09.006.

(50) Nissim, R.; Batchelor-McAuley, C.; Li, Q.; Compton, R. G. The Anthraquinone Mediated One-Electron Reduction of Oxygen in Acetonitrile. *J. Electroanal. Chem.* **2012**, *681*, 44–48. https://doi.org/10.1016/j.jelechem.2012.06.001.

(51) Jeziorek, D.; Ossowski, T.; Liwo, A.; Dyl, D.; Nowacka, M.; Woźnicki, W. Theoretical and Electrochemical Study of the Mechanism of Anthraquinone-Mediated One-Electron Reduction of Oxygen: The Involvement of Adducts of Dioxygen Species to Anthraquinones. *J. Chem. Soc., Perkin Trans. 2*, **1997**, 229-236. https://doi.org/10.1039/a605549d.

(52) Kuivila, H. G. Electrophilic Displacement Reactions. VI. Catalysis by Strong Acids in the Reaction between Hydrogen Peroxide and Benzeneboronic Acid. *J. Am. Chem. Soc.* **1955**, *77* (15), 4014–4016. https://doi.org/10.1021/ja01620a017.

(53) Debardieux, L. Organic and Biological Chemistry. *Biochimie* **2003**, *85* (5), 563. https://doi.org/10.1016/s0300-9084(03)00010-5.

(54) Lu, C.; Lin, C.; Chang, C.; Wu, S.; Lo, L. Nitrophenylboronic Acids as Highly Chemoselective Probes To Detect Hydrogen Peroxide in Foods and Agricultural Products. *J. Agric. Food Chem.* **2011**, 11403–11406.

(55) Smidt, E.; Meissl, K. The Applicability of Fourier Transform Infrared (FT-IR) Spectroscopy in Waste Management. *Waste Mangement.* **2007**, *27*, 268–276. https://doi.org/10.1016/j.wasman.2006.01.016.

(56) Valarmathi, T.; Premkumar, R.; Benial, A. M. F. Spectroscopic and Molecular Docking Studies on 1- Hydroxyanthraquinone : A Potent Ovarian Cancer Drug. *J. Mol. Struct.* **2020**, *1213*, 128163. https://doi.org/10.1016/j.molstruc.2020.128163.

(57) De Clerck, K.; Rahier, H.; Mele, B. Van; Westbroek, P.; Kiekens, P. Dye – Fiber Interactions in PET Fibers : Hydrogen Bonding Studied by IR-Spectroscopy. *Journal of applied polymer science.* **2007**. https://doi.org/10.1002/app.

(58) Upadhyaya, H. P. Ground-State Intramolecular Proton Transfer and Observation of High Energy Tautomer in 1,4-Dihydroxyanthraquinone. *J. Mol. Struct.* **2021**, *1232*, 130050. https://doi.org/10.1016/j.molstruc.2021.130050.

(59) Kizior, B.; Panek, J. J.; Szyja, B. M. Structure-Property Relationship in Selected Naphtho- and Anthra-Quinone Derivatives on the Basis of Density Functional Theory and Car – Parrinello Molecular Dynamics. *Symmetry.* **2021**, *13*(4), 564. https://doi.org/10.3390/sym13040564.

(60) Ajloo, D.; Yoonesi, B.; Soleymanpour, A. Solvent Effect on the Reduction Potential of Anthraquinones Derivatives. The Experimental and Computational Studies. *Int. J. Electrochem. Sci.* **2010**, *5* (4), 459–477.

(61) Babaei, A.; Connor, P. A.; McQuillan, A. J.; Umapathy, S. UV-Visible Spectroelectrochemistry of Reduction Products of Anthraquinone in Dimethylformamide Solutions: An Advanced Undergraduate Experiment. *J. Chem. Educ.* **1997**, *74* (10), 1200–1203. https://doi.org/10.1021/ed074p1200.

7. List of Tables

8. List of Figures